Journal of Medicinal Chemistry

Article

Discovery of Small-Molecule Inhibitors of Ubiquitin Specific Protease 7 (USP7) Using Integrated NMR and In-Silico Techniques

Paola Di Lello, Richard Pastor, Jeremy M. Murray, Robert A. Blake, Frederick Cohen, Terry D Crawford, Joy Drobnick, Jason Drummond, Lorna Kategaya, Tracy Kleinheinz, Till Maurer, Lionel Rouge, Xianrui Zhao, Ingrid Wertz, Chudi Ndubaku, and Vickie Tsui

J. Med. Chem., **Just Accepted Manuscript** • DOI: 10.1021/acs.jmedchem.7b01293 • Publication Date (Web): 22 Nov 2017

Just Accepted

ACS Publications

Journal of Medicinal Chemistry is published by the American Chemical Society. 1155 Sixteenth Street N.W., Washington, DC 20036

Discovery of Small-Molecule Inhibitors of Ubiquitin Specific Protease 7 (USP7) Using Integrated NMR and In-Silico Techniques

Paola Di Lello, [†‡*] *Richard Pastor,* [†‡*] *Jeremy M. Murray,* [†] *Robert A. Blake,* [†] *Frederick Cohen,* [†] *Terry D. Crawford,* [†] *Joy Drobnick,* [†] *Jason Drummond,* [†] *Lorna Kategaya,* [†] *Tracy Kleinheinz,* [†] *Till Maurer,* [†] *Lionel Rougé,* [†] *Xianrui Zhao,* [†] *Ingrid Wertz,* [†] *Chudi Ndubaku,* [†] *Vickie Tsui*[†*]

[†]Genentech, Inc. 1 DNA Way, South San Francisco, California 94080, United States

ABSTRACT

USP7 is a deubiquitinase implicated in destabilizing the tumor suppressor p53 and for this reason it has gained increasing attention as a potential oncology target for small molecule inhibitors. Herein we describe the biophysical, biochemical and computational approaches that led to the identification of 4-(2-aminopyridin-3-yl)-phenol compounds described by Kategaya *et al.*[1] as specific inhibitors of USP7. Fragment based lead discovery (FBLD) by NMR combined with virtual screening and re-mining of biochemical high-throughput screening (HTS) hits led to the discovery of a series of ligands that bind in the "palm" region of the catalytic domain of USP7 and inhibit its catalytic activity. These ligands were then optimized by structure-based design to yield cell-active molecules with reasonable physical properties. This discovery process not only

involved multiple techniques working in concert, but also illustrated a unique way in which hits from orthogonal screening approaches complemented each other for lead identification.

INTRODUCTION

Ubiquitination is a key form of post-translational modification. Ubiquitination largely targets protein substrates for degradation by the 26S proteasome in a tightly regulated manner [2]. As such, ubiquitination involves substrate-specific ubiquitin ligases (E3) that catalyze the formation of an isopeptide bond between the carboxyl-terminus of ubiquitin and the lysine side-chain of the target protein [3]. A ubiquitin monomer can be attached via this mechanism to a protein substrate, and multiple ubiquitins can be linked to each other resulting in polyubiquitination. Depending on the type of linkage between the ubiquitin molecules in these chains, polyubiquitination can serve as a signal for degradation of the protein substrate [4-5].

Opposing the function of these E3 are deubiquitinating enzymes, or DUBs. As the name suggests, a DUB removes ubiquitin from a protein substrate, another ubiquitin within a polyubiquitin chain, or a ubiquitin precursor. There are around 100 known human DUBs, consisting of five major families: Ubiquitin-Specific Proteases (USPs), Ubiquitin Carboxyl-terminal Hydrolases (UCHs), Ovarian Tumor proteases (OTUs), Machado-Joseph Disease protein domain proteases (MJDs) and JAMM/MPN domain-associated metallopeptidases (JAMMs) [6]. In addition, two families of DUBs have been recently discovered, the Monocyte Chemotactic Protein-Induced Proteins (MCPIPs) [7-8] and a new class of cysteine proteases belonging to the MINDY family (MIU-containing novel DUB family) [9]. USPs are the largest

family of DUBs [8] and members of this family are cysteine proteases that rely on a "catalytic triad" of cysteine, aspartic/glutamic acid and histidine to hydrolyze the isopeptide bond.

Several USPs have been reported to play important biological roles that make them attractive as therapeutic targets [10-11]. An example is USP7 or herpes virus associated USP (HAUSP), which is considered a potential oncology target due to its role in the destabilization of the tumor suppressor p53 [12]. As a transcription activator, p53 modulates the expression of genes like p21, Bax, or Puma that control cell cycle arrest or apoptosis in response to various cellular stresses [13]. However, in the majority of human cancers p53 is inactivated by either mutations in p53 itself or alterations in the pathways that regulate its levels [14-15]. Deubiquitination of MDM2, a substrate of USP7 and itself a ligase for p53, is one of the mechanisms by which wild-type p53 is inactivated. Therefore, inhibition of USP7 can tip the balance towards ubiquitinated MDM2, thus triggering its degradation and reactivating the p53 pathway in cancer cells that retain wild-type p53.

We recently reported a new class of highly selective USP7 inhibitors, **28** (GNE-6640) and **27** (GNE-6776), which modulated the enzymatic activity of USP7 by binding to a novel functional site within the "palm" region of the enzyme and interfering with substrate binding [1]. In this manuscript we describe the structure-based drug discovery strategies that led to the identification of the aforementioned new functional site on USP7 and to the discovery of the "palm" compounds. The discovery process that led to this new class of USP7 inhibitors involved the interplay between biochemical, in-silico and biophysical techniques, including Nuclear Magnetic Resonance (NMR) and crystallography. In addition, hits from multiple small molecule libraries (fragment, HTS and sample management libraries) were combined to generate this novel series. The detailed account of how the techniques and libraries complemented each other, as well as the

structure-based optimization leading to molecules with improved biochemical potency, and observable cellular activity will be presented.

RESULTS

Discovery, biophysical characterization and structure-based optimization of the oxadiazole series.

We have applied different screening approaches (a fragment screen by NMR and a full HTS campaign) to search for small molecule ligands that would specifically bind and inhibit the catalytic domain of USP7 [1]. In particular, a fragment screen by NMR led to the discovery of a series of small molecules that bind in the active site near the catalytic cysteine (Cys223), and were further developed into moderately active inhibitors of the enzymatic activity (unpublished results). In a parallel approach we also used computational methods to look for additional scaffolds that could bind in the enzyme active site and potentially block its activity. Compound **1** (Table 1), a fragment-screen hit that binds in the enzyme active site, was used as the query molecule to carry out ligand-based virtual screening against compounds in the Genentech internal sample management library. The 500 top-scoring hits from the virtual screen were then analyzed by visual inspection, leading to the selection of twenty-one compounds. To verify that these twenty-one compounds bound to the catalytic domain of USP7 (USP7-CD) we tested them by NMR using Saturation Transfer Difference (STD) experiments. Although many of these molecules did not confirm as ligands, a smaller subset of twelve compounds showed binding to USP7-CD. These twelve compounds were then evaluated for biochemical activity and, to further characterize their binding site, they were also tested in NMR titration experiments with labeled USP7-CD. Addition of each of these hits to labeled USP7-CD induced chemical shifts

perturbations and/or line broadening of signals in the two-dimensional [^{1}H -^{15}N]-TROSY spectrum of labeled USP7-CD, confirming an interaction with the protein. However, of the twelve compounds tested with labeled USP7-CD, three induced unspecific signals line broadening suggesting possible protein aggregation, whereas five appeared to bind in more than one site; in fact they caused changes in the resonances of residues located in the active site as well as in other regions of the protein. The remaining four compounds (**2-5)** induced chemical shifts perturbations only in a select subset of NMR signals, suggesting they interacted with USP7-CD at a specific site (Figure 1B). These four hits, all of which contained an oxadiazole core with a 4-phenol on one side and piperidine or pyrrolidine on the other side, were the only ones of the twelve tested that had detectable biochemical activities (Table 1).

Surprisingly, the chemical shifts perturbations that **2** and its three analogs (**3-5**) induced on labeled USP7-CD (Figure 1B) also involved a different subset of peaks from that observed for the active site ligand **1** (Figure 1A), thus pointing to a different binding site on the protein surface. Nevertheless, the KD values of **2** and **3**, estimated by NMR to be in the range 12-27 μM for USP7-CD, were within 5 fold of the biochemical IC_{50}'s determined for full length USP7 (Table 1).

In the case of the active site ligand **1** the amino acids showing the largest chemical shifts perturbations upon addition of the ligand to labeled USP7-CD were Met292, Gln293, His294, Asp295 (located in the switching loop), Met410, Phe411, Asp412, Asn418, Ile419, Lys420, Ile421 (located in the β0-β0' sheet) and Gly458, Asp459, Asn460, Gly462, Gly463, His464 (located in the loop connecting strands β10 and β11). When mapped onto the structure of apo USP7-CD, these amino acids clearly defined a ligand binding site (Figure 1C) that overlapped with the catalytic site. On the contrary in the case of **2** the largest chemical shifts perturbations

and/or signals line-broadening were observed for a different set of amino acids, namely Ile320, Lys322 (helix α6), Gly326, Met328 (strand β1), Ile350, Gln351, Leu352, Ser353 (strand β3), Tyr347, Tyr348, Asp349 (located in the loop connecting strands β2 and β3), His403, Met407 (strand β8), Asp295, Gln297, Glu298, Cys300, Arg301, Leu304, Asp305, Val307, Glu308 (helix α5), and Lys281, Gly284, Trp285. When mapped onto the structure of apo USP7-CD, these amino acids clustered within the "palm site" of USP7-CD, in a region adjacent to the catalytic site (Figure 1D), thus revealing a novel functional site.

The location of the binding site identified by the NMR chemical shift perturbation studies was consistent with the crystal structure of the USP7-CD/**2** complex that was subsequently determined. The structure also revealed several critical interactions between ligand and protein. The phenol ring was buried in a hydrophobic pocket with an edge-to-face interaction with Phe324 and the phenol hydroxyl engaged in a hydrogen bond interaction with His403 (Figure 2). While the oxadiazole moiety was partially solvent exposed, it was involved in a face-to-face π-stacking interaction with Tyr348. The piperidine was, for the most part solvent exposed, and based on the electron density, was not involved in any interactions with the protein. SAR on the piperidine (Table 1) indicated that it made minimal contribution to activity.

To follow up on **3**, analogues were designed and prioritized based on the crystal structure (Table 2). Replacement of the oxadiazole core with a 2,4 substituted oxazole (**6**) resulted in no change in activity. However, employing a 2,5-substituted oxazole (**7**) led to a 3-fold potency increase. For **7** the oxygen (rather than the nitrogen in **6**) in the oxazole is closer in space to the methylene part of the Arg301 sidechain and this potentially leads to a better Van der Waals interaction because of the smaller negative dipole of the oxygen relative to the nitrogen. An

additional 2-fold increase in activity was observed when phenol was replaced by 3-fluorophenol, likely due to increased phenol acidity or slight changes in conformational preference (Figure S1).

Discovery and characterization of the aminopyridine series.

Having discovered that the "palm" region of USP7-CD contains an additional functional site that could be exploited to modulate the enzymatic activity through small molecules binding, we applied an NMR driven scaffold-hopping strategy to search for structurally novel compounds that could bind to this site and potentially be developed into selective USP7 inhibitors.

Instead of generating structurally novel compounds through a computational approach to scaffold hopping, we re-mined the hits from our original NMR fragment screen, searching for ligands that had a binding fingerprint on labeled-USP7 similar to that observed for **2** and its analogs. Using this approach we were able to identify several heterocyclic-substituted phenols (i.e. aminopyridine-phenols and aminopyrazine-phenols, Figure 3A) that showed perturbation maps remarkably similar to those observed for **2** (Figure 3B-C), suggesting that they bind USP7-CD in the same site and possibly with the same binding pose as compounds of the oxazole series.

Interestingly, the aminopyridine-phenol motif found in some of the hits from the fragment screen was also present in **14** and **15**, two of the 76 hits from the high-throughput screening (HTS) (Table 3) of Genentech proprietary library of ~2 million compounds. However, these two HTS hits had been previously de-prioritized for re-confirmation in favor of hits that were commercially available and significantly more potent [1].

Efforts that led to the re-synthesis of compounds **14** and **15** also produced compound **16** as a synthetic by-product and all three compounds demonstrated micromolar biochemical activities (Table 3). A co-crystal structure of **16** was obtained and it showed that the compound bound in a similar mode to that of **3**, as both occupied the same "palm" binding site, where significant

affinity was gained by engaging His403 and Phe324 with a phenol moiety (Figure 4A). However, electron density for the other components of the ligand were not well-defined, leaving its exact binding mode undetermined. Instead, four binding modes were possible based on the observed electron density as shown in Figure 5, with each binding mode having a distinct orientation of the solvent-exposed phenol and the amino moiety. Modeling and occupancy refinement of multiple possible binding orientations also revealed an unoccupied hydrophobic pocket, proximal to the ligand, which was targeted for affinity optimization (Figure 4B). Initial medicinal chemistry efforts focused on both affinity optimization and elucidation of the inhibitory binding mode.

Attempts to optimize **16** began by substituting at the 2, 4 and 6 positions of the central pyridine ring (Table 4). Deletion of the 2-amino moiety (**17**) led to a complete loss in activity, while addition of a 6-amino group (**18**) showed comparable activity. Appending an ethyl at C4 (**20**) led to a five-fold activity increase, whereas propyl was too long for the small pocket (**21**). C4-isopropyl was five-fold less active than C4-ethyl (**22** vs. **20**) and C4-cyano (**23**) led to complete loss of activity. This preference for small, unbranched hydrophobic groups in the C4 position was consistent with two of the possible ligand binding modes (Figure 5, C and D).

C3 and C5 analogue synthesis was undertaken, where one of the goals was to identify which phenol moiety made the critical His403 interaction (Table 5). The resulting SAR is shown in Table 5 and unexpectedly, the SAR at both positions was very similar. At both positions, phenyl substitution led to a moderate reduction in activity, cyanophenyl substitution was well tolerated, and indazole substitution improved activity by several fold, resulting in the most active compounds from this series. In addition, the observation that compounds without a phenol in C3 or C5 (Table S1) were significantly less potent demonstrated that a phenol was required for

detectable activity. Taken together, the results suggested the latter two conformations in Figure 5 C or D could be adopted to place phenol in the His403 pocket.

Cell-based assay results.

A representative set of our most biochemically potent and chemically diverse compounds was tested in a MDM2 MSD cell-based assay with SJSA cells, which are osteosarcoma cells with high level of MDM2 expression[16], to study their effects on levels of ubiquitinated MDM2 vs the total amount of MDM2 in a dose-response fashion (Table 6). The rank order of activities corresponded well with biochemical potency. Compound **28** demonstrated sub-micromolar activity and was the most potent analog of this group, consistent with its relative biochemical activity. Compound **27** demonstrated single digit micromolar activity, while **18** and **31** both were an order of magnitude less active. The negative control **29** had EC_{50} >50 μM.

Compounds **18**, **27** and **28** were further tested in EOL-1 cells alongside **29** as a negative control (NC). These compounds were selected based on their EC_{50} values in the MDM2 MSD assay. The effects of these compounds on the levels of proteins downstream of the USP7/MDM2 pathway (Figure 6A) were examined at 1.3 μM and 5 μM by Western Blots (Figure 6B). Using tubulin as a loading control, the normalized levels of p53 and p21 were quantitatively compared to DMSO and plotted in Figures 6C and 6D, respectively. As expected, the negative control had minimal effect on the levels of p53 and p21, whereas compounds **27** and **28** showed a significant increase in p53 levels. Compounds **27**, **28**, and to a lesser extent **18**, also up-regulated p21.

Furthermore, the effects of USP7 inhibitors on the viability and caspase activity of EOL-1 cells were examined (Fig. 7A-B) using imaging techniques. The percent confluence measured the area of each well occupied by cells, and dose-dependent decrease in cell viability was observed

over 48 hours when treated with each of the active inhibitors while treatment with the negative control did not have significant effects. Caspase activity was increased and the effects were dose-dependent following treatment with **18** and **28** over 48 hours, whereas all doses resulted in minimal effects on caspase activation for the negative control arm. This dose-dependent effect on caspase activity was lower for **27**, leading to the hypothesis that **28** decreases cell viability via both apoptosis and cell cycle arrest (Figure 6A), whereas **27** mainly causes cell cycle arrest. Cell cycle arrest is generally triggered first in response to an insult, followed by induction of apoptosis in case the cell damage cannot be repaired. Therefore, treatment with a more potent compound like **28** can lead to apoptosis in addition to cell cycle arrest, whereas treatment with a less potent compound like **27** would mainly trigger cell cycle arrest. For compound **18**, which is the least potent in inhibiting USP7 (Table 4 and Table 6) and in modulating the levels of p53 and p21 (Figure 6C-D), the observed increase in caspase activity (Figure 7B) and the resulting decrease in cell viability (Figure 7A) could be due to off-target effects.

This hypothesis can also explain the CellTiter-Glo results (Figure 7C) measuring ATP levels at the 48-hour end point. Unlike the negative control, all three inhibitors led to decreased ATP levels as their concentrations were increased. Compound **28** was more potent, while the effects of **27** were seen at higher inhibitor concentrations. As expected, the negative control had minimal effects.

There are several reports of closely related analogs being kinase inhibitors [17-19] and to assess potential contributions of off-target kinase activity to the cellular phenotypes that were observed, **27** and **28** were profiled against a kinase panel consisting of 219 kinases. We observed only modest inhibition, with IC_{50} values in the low micromolar to sub-micromolar range, against 6 kinases (data not shown). Most importantly, **27** and **28**, our most potent compounds, as well as

the negative control **29** were equipotent against all of these kinases, suggesting that kinase-inhibitory effects did not contribute to effects on cellular viability. This conclusion is further supported by published studies[1] demonstrating that **28** and **27** are on-pathway, USP7-selective inhibitors. Both compounds reduce cell viability in wild type HCT-116 cells but not in USP7-null HCT-116 cells indicating that USP7 expression is required for cellular activity. Furthermore **27**, **28**, and **29** were all profiled in 3- and 5-day viability assays in large panels of cell lines. While **27** and **28** significantly reduced viability of a number of cell lines, **29** was inactive in all cell lines evaluated. Collectively, these data indicate that the modest *in vitro* kinase inhibition observed for our USP7 inhibitors does not translate to cellular activity."

Chemistry

The oxadiazoles and oxazoles shown in Tables 1 and 2 were prepared using a suite of heterocycle-forming reactions in both a convergent and linear manner (Schemes 1 – 3). Condensations between acid and hydroxyamidine components promoted by carbonyl diimidazole (CDI) led to the described oxadiazoles. The acid components were commercially sourced whereas the hydroxyamidine coupling partners were formed from nitrile precursors.

The 2,4 substituted oxazoles were generated from convergent couplings between corresponding commercially available α-bromo-ketones and amide monomers. On the other hand, the 2,5 substituted oxazoles resulted from a linear sequence which began with addition of nitromethane to N-Boc-piperidine aldehyde to afford the 2-nitro-alcohol. Nitro reduction, amine acylation, and alcohol oxidation affords the β-acylamino-ketone which was then cyclized under Burgess reagent promoted conditions to form the oxazole ring.

Preparation of the bis-phenol substituted aminopyridines shown in Table 4 utilized a bis-bromination with NBS followed by a bis-Suzuki coupling with 4-anisole boronic acid on the corresponding pyridine precursors (Scheme 4). Methoxy demethylation with BBr_3 then affords **17** – **23**.

Synthesis of both the C3 and C5 phenol replacements in the aminopyridine core both involved conducting Suzuki couplings on the corresponding bromo-aminopyridine late-stage intermediates **50** and **55** (Schemes 5 and 6).

Synthesis of **50** began with bis-bromination of commercially available 4-ethyl-aminopyridine followed by selective debromination at the more labile C5 position to afford **47**. Suzuki coupling to install a 4-methoxy-phenyl group at C3 followed by C5 bromination and methoxy demthylation with HBr affords **50**.

Synthesis of **55** began with selective C5 bromination of 4-ethyl-aminopyridine with NBS. Installation of the 4-MeO-Phenyl group by Suzuki coupling followed by C3 bromination and methoxydemthylation then affords **55**.

DISCUSSION AND CONCLUSIONS

Herein, we describe the details of how the USP7 tool compounds **27** and **28** reported in Kategaya *et al*. [1] were discovered. These are the first small molecule allosteric inhibitors of any USPs that have been fully characterized using biophysical and biochemical methods as well as cell-based assays. The lack of comprehensive data in past publications represents both the novelty and challenge of this target class[20], and we could show that by combining experimental and computational methods with a variety of chemical libraries we were able to discover these "palm" site binding series.

NMR played a significant role in the discovery of lead matter, and it is no surprise that our lead matter came from a biophysical screen, since a cysteine protease like USP7 could turn up many reactive false positives in a biochemical HTS campaign. In fact, the HTS hits that were followed up by re-mining efforts described in this publication progressed farther than other HTS series. Most of the biochemical HTS hits failed to confirm upon re-synthesis, did not show specific activity to the catalytic domain, or were shown to be potential aggregators. Furthermore, none of the hits from the biochemical HTS were successful in co-crystallization studies, hindering rational structure-based design[1].

Our discovery process started with the application of a shape-based virtual screen using the active-site binder as a query molecule against compounds in the Genentech internal sample management library. Combining this virtual screen with a comprehensive biophysical and biochemical characterization of the virtual hits was a critical step in the discovery process. It allowed us to identify a structurally unique chemical series, the oxadiazole series, and most importantly it unveiled the presence of a second functional site, the "palm" site, besides the catalytic site. The subsequent approach of re-mining the NMR fragment hit set for additional scaffolds with similar binding fingerprints to the oxadiazole compounds but with different chemical structures was key in turning out several hits containing the aminopyridine and aminopyrazine substructures. Even though these fragment hits were not potent enough to observe biochemical activity, taking the chemical moiety back to re-examine the deprioritized HTS hits led to the successful discovery of our most potent series, the aminopyridine series.

Not only were crystal structures important in the lead discovery stage, they were also essential for optimization of the aminopyridine series. Even though the electron densities provided multiple possible binding modes, medicinal chemistry optimization helped to narrow down the

binding modes to two possibilities. During this process, the ethyl group was installed in a small hydrophobic pocket in the 4-position of the aminopyridine to boost potency, and unsubstituted indazoles at either the C3 or C5 position of the aminopyridine were found to be most active, when coupled with a phenol on the other side. Compounds with measurable cellular EC_{50} were obtained, and they had excellent DUB selectivity as described in Kategaya *et al*. [1]. Furthermore, compounds were shown to upregulate p21 and p53 in EOL-1 cells in a dose-dependent manner, in agreement with the pathway biology of inhibiting USP7. Increase in caspase activity and decreased cell viability were also observed, consistent with the expected outcome of USP7 inhibition.

In order to progress this series as a clinical candidate, the key challenges will be to improve cellular potency and plasma protein binding properties while maintaining good pharmacokinetics. **27** demonstrated good oral bioavailability and half-life in mice, but only transiently achieved target plasma exposures, due to its high plasma protein binding and lack of sub-micromolar cellular EC_{50}.[1] Therefore, improving both these parameters will enhance the ability of this series to achieve efficacious concentrations *in vivo*. In addition, profiling of this series in both *in vitro* and *in vivo* toxicity assays would be required to identify potential negative side effects.

Our experience here provides a lesson for identifying lead matter for challenging targets such as DUBs, in that an integrated approach is crucial and involves multiple biophysical, biochemical and *in silico* techniques, as well as a variety of compound libraries, which normally would be studied separately. The process we described to re-mine hits with various techniques and from different hit sets, as opposed to more traditional drug discovery efforts, can improve

the chance of identifying potent inhibitors of new classes of enzymes and proteins otherwise considered undruggable.

EXPERIMENTAL SECTION

Ligand-based virtual screening

Ligand-based virtual screening was carried out using fastROCS (OpenEye, Inc. www.eyesopen.com) as implemented at Genentech. The specifics of the integration of fastROCS with a variety of databases have been described [21]. Compound **1** was used as the query molecule against a proprietary library of ~100,000 compounds in Genentech's sample management, and a maximum of 500 top-scoring compounds using default parameters were returned without post-clustering. Visual inspection was carried out with consideration of lead-likeness as well as dry powder availability.

Protein expression and purification for NMR

The catalytic domain of USP7 (USP7-CD), encompassing residues 208-554, was expressed as a His-Tag fusion protein in *E. coli* Rosetta 2 (DE3) cells. Unlabeled USP7-CD was produced according to the protocol reported elsewhere.[22] Uniformly ([^{15}N-^{13}C-^{2}H], δ1[$^{13}CH_3$]-Ile, [$^{13}CH_3$]-Leu/Val and [$^{13}CH_3$]-Met)-labeled USP7-CD was expressed and purified as previously described.[23]

Samples for NMR

The Genentech fragment library was screened as reported elsewhere [1].

Samples for binding validation by Saturation Transfer Difference (STD) experiments contained 250 μM of ligand and 5μM of unlabeled USP7-CD in NMR buffer [PBS (pH 7.4) in 100% D_2O, 50 μM 4,4-Dimethyl-4-Silapentane-1-Sulfonic acid (DSS).

Samples for binding site mapping consisted of 250-340 μM of labeled USP7-CD in PBS (pH 7.4), 300 μM-2.5 mM of ligand, 1 mM TCEP-d_{16}, 10% D_2O and up to 2.5% DMSO-d_6.

For the determination of the binding constants, each sample consisted of 270 μM of isotopically labeled USP7-CD in PBS (pH 7.4), 1 mM TCEP-d_{16}, 10% D_2O and up to 2.5% DMSO-d_6. Individual ligands were added to the protein sample stepwise, over a range of increasing concentrations [250μM, 500 μM, 1000 μM, 2000 μM and 4000 μM].

NMR experiments and data analysis

NMR experiments were performed on 500 MHz and 600 MHz spectrometers equipped with 1.7 mm and 5 mm cryoprobes, respectively.

The backbone resonances assignment for labeled USP7-CD was obtained as previously reported [23]. Chemical shifts of the proton, carbon and nitrogen nuclei were referenced externally to that of DSS at 0 ppm.

The fragment library was screened using Saturation Transfer Difference (STD) experiments [24] run at 280 K. Hits from the primary screen were further characterized by analyzing the ligand-induced chemical shifts changes of labeled USP7-CD in [^{1}H-^{15}N]-TROSY experiments [25]

STD experiments were processed and analyzed using TOPSPIN 3.0. Data collected for binding site mapping were processed with NMRPipe/NMRDraw [26] and analyzed with NMRView [27].

The dissociation constants (KD) were derived from the ^{1}H and ^{15}N chemical shifts changes observed in the [^{1}H-^{15}N]-TROSY spectra of isotopically labeled USP7-CD upon addition of increasing amounts of ligand. Chemical shift changes, measured at various protein/ligand ratios, were plotted as function of the ligand concentration, and then fitted according to the equation:

$$\Delta\delta = \Delta\delta_{max}\frac{K_D + [P] + [L] - \sqrt{(KD + [P] + [L])^2 - 4[P][L]}}{2[P]}$$

where $\Delta\delta$ is the chemical shift change at various protein/ligand ratios, $\Delta\delta_{max}$ is the chemical shift change at saturation, KD is the dissociation constant, and [L] and [P] are the ligand and protein concentrations, respectively.

Biochemical assays

Biochemical USP7 assays used Ubiquitin-Rho110 as a substrate. The reaction buffer consisted of 50 mM Tris (pH 7.5), 0.01%(v/v) Triton X-100, 2.5 mM Dithiothreitol, 0.1% (w/v) bovine gamma globulin (Sigma cat # G5009-25G); USP7, full-length, native C-Terminus, 0.2 nM; the substrate, Ubiquitin-Rho110 (Boston Biochem cat # U-555), 1 μM. Reactions were carried out for 1 hour at room temperature, in black 20μL volume polystyrene ProxiPlate 384 F Plus (PerkinElmer cat # 6008260).

Test compounds, including a control USP7 inhibitor (Ub-aldehyde, Boston Biochem cat # U-201) were serially diluted in DMSO, in 384-well clear V-bottom polypropylene plates (Greiner cat # 781280). Compounds in DMSO were diluted 10-fold into Reaction Buffer, to achieve 3-fold the final desired concentration. The substrate, Ubiquitin-Rho110 (Boston Biochem cat # U-555), was prepared at 3 μM (3-fold the final concentration) and 5 μl was dispensed into the reaction plate. 5 μl of the compounds (diluted in reaction buffer at 3-fold the final concentration) were transferred to the reaction plate. 5 μl of 0.6 nM USP7 (diluted in reaction buffer at 3-fold the final concentration) was transferred to the reaction plate to initiate the reaction. After 1 hour incubation at room temperature the reaction was quenched by the addition of 5 μl of 400 mM acetic acid. The enzymatic product was measured by quantifying the fluorescence signal of cleaved Rhodamine-110 using excitation at 485 nm and emission at 535 nm. When pre-incubation of USP7 with compounds was required, the order of addition of reagents was

modified to pre-mix the compounds with USP7 (with a 1 hour incubation period), prior to the addition of the substrate and the initiation of the reaction period. Percentage inhibition values were calculated relative to a no enzyme control and an uninhibited enzyme control. Curve fitting and IC_{50} calculations were carried out using Genedata Screener software.

Crystallization and data collection

Crystals were grown by the hanging-drop method by mixing the USP7 catalytic domain (residues 208–554) at 15 mg/ml with an equal volume of reservoir solution containing 100 mM Tris,-HCl, pH 7.0, and 20% PEG1000 (v/v). Co-structures with compounds were obtained by soaking crystals with 1 mM of compound overnight. Crystals were cryoprotected with reservoir solution supplemented with 20% glycerol (v/v) and flash frozen in liquid nitrogen. Data collection and refinement statistics are detailed in Table S2.

MDM2 MSD cell-based assays

SJSA cells were maintained in RPMI media containing 10% FBS (Sigma Aldrich, cat #F6765) and 1% GlutaMAX (ThermoFisher, cat #35050061). SJSA cells were seeded at 120,000 cells per well in 90 µ l of low serum RPMI supplemented with 0.5% FBS and 1% GlutaMAX into a 96 well TC-treated plate (Greiner cat #655090). Cells were allowed to attach to the plate for 2 hours at 37 °C.

Test compounds were serially diluted in DMSO, in a 96 well clear V-bottom polypropylene plate (Greiner, cat #651261). 5 µl of compound diluted in DMSO was added to an intermediate plate containing 95 µl/well of low serum media per well of a 96-well clear V-bottom polypropylene plate. 10 µl of intermediate dilution of compound in media were added to cell plate yielding a 1:200 final dilution of test compound. Cell plates were incubated with compound at 37 °C with 5% CO_2 overnight for 16 hours.

After compound incubation 20 μM final concentration of MG132 (Cayman Chemical, Cat#10012628) was added to cell plate. Plates were incubated at 37 °C for 1 hour.

Lysis buffer was prepared per vendor instructions. 15 μl per well 5x cold lysis buffer was added to cell plates and incubate on a shaker at 4 °C for 30 mins.

The 96-well MSD plates provided in Ubiquitinated, Total MDM2 MULTI-SPOT 96-Well 4 spot Plate Kit (Cat#N45168B-1; Meso Scale Discovery, Gaithersburg, MD) were prepared by incubation with 150μL/well of 3% Blocker Buffer A (Meso Scale Discovery Cat# R93BA-4) in 1X MSD Tris Wash Buffer (Meso Scale Discovery Cat# R61TX-1) for 1h. The plate was washed 3 times with Tris Wash buffer.

100 μl of cellular lysate was transferred to each of the MSD Assay plate.

Cell lysates were incubated in plate for 1 hour at room temperature while shaking (650 rpm) in the dark.

The MSD plates were washed 3 times with 1×Tris wash buffer (Meso Scale Discovery) then incubated with 25 μL of 1X SULFO-TAG Anti-Total MDM2 Antibody in antibody buffer containing blockers specified in manufacturer protocol. Antibody was incubated in plates for 1 hour at room temperature while shaking (650 rpm) in the dark.

The MSD plates were washed 3 times with 1x Tris Wash buffer.

150 μl microliters of 1×read buffer T with surfactant (Meso Scale Discovery) was added to the plate and the relative light units (RLU) were recorded in a Sector Imager 6000 (Meso Scale Discovery). Dose response of compound induced changes to Ratio of ub-MDM2/Total MDM2 was fit using Genedata Screener software.

Cell viability assays

EOL-1 cells were maintained in RPMI media containing 10% FBS. 15,000 cells were seeded in 1-well of a 96-well plate (Corning cat # 3904). Cells were treated immediately or the next day and then monitored for 48h via live imaging using an Incucyte instrument. To monitor caspase activity, 2 μM CellEvent Caspase 3/7 reagent (Life Technologies cat # C10423) was added to seeding media. Scans were collected every 3 h, using a 4X objective. Phase contrast was used to measure cell confluence while green fluorescence was used to measure caspase activity. The images were analyzed using IncuCyte software (Basic Analysis parameters). All treatments were done in triplicate. 48 h after imaging, CellTiter-Glo reagent (Promega cat # G7570) was added to each well as an independent measure of number of remaining cells at the end of the experiment. CTG reagent was added following the vendor protocol.

Western blots

A total of $5x10^6$ cells were seeded into 1 well of a 12-well plate and treated with DMSO, 1.3 μM or 5 μM cmpds, for 4 h prior to lysis for Western Blot analysis. Blots were scanned and analyzed using a Licor technology. Antibodies used: USP7 (Abcam cat # ab84098), MDM2 (Santa Cruz cat # sc-965), tubulin (Licor cat # 926-42211), p53 (Thermo Scientific cat # MS738-P1), p21 (Millipore cat # 05-655).

Synthesis

General Methods. All solvents and reagents were used as obtained. NMR analysis performed in deuterated solvent on Bruker Avance 400- or 500-MHz NMR spectrometers. The spectra were referenced internally to tetramethylsilane (TMS). Chemical shifts are reported in ppm (δ) (in the NMR description, s = singlet, d = doublet, t = triplet, q = quartet, m = multiplet, and br = broad peak). All coupling constants (J) are reported in Hertz. Mass spectra were measured with a Finnigan SSQ710C spectrometer using an ESI source coupled to a Waters 600MS high

performance liquid chromatography (HPLC) system operating in reverse-phase mode with an X-bridge Phenyl column of dimensions 150 mm by 2.6 mm, with 5 mm sized particles. Preparatory-scale silica gel chromatography was performed using medium-pressure liquid chromatography (MPLC) on a CombiFlash Companion (Teledyne ISCO) with RediSep normal phase silica gel (35−60 μm) columns and UV detection at 254 nm. Reverse-phase (HPLC) was used to purify compounds as needed by elution from a Phenomenex Gemini-NX C18 column (20.2 × 50 mm, 5 micron) as stationary phase using mobile phase indicated, and operating at a 35 mL/min flow rate on a Waters 3100 mass-directed prep instrument. Chemical purities were >95% for all final compounds as assessed by LC/MS analysis. The following analytical method was used to determine chemical purity of final compounds: HPLC-Agilent 1200, water with 0.05% TFA, acetonitrile with 0.05% TFA (buffer B), Agilent SB-C18, 1.8 mM, 2.1 x 30 mm, 25 ºC, 3–95% buffer B in 8.5 min, 95% in 2.5 min, 400 mL/min, 220 nm and 254 nm, equipped with Agilent quadrupole 6140, ESI positive, 90-1300 amu.

Example 1 was obtained from Sigma-Aldrich (catalog # CDS002148). ^{1}H NMR (400 MHz, DMSO-d6) δ 8.87 (s, 2H), 7.31 (td, *J* = 8.4, 7.2 Hz, 1H), 6.87 – 6.71 (m, 3H), 3.88 (d, *J* = 6.3 Hz, 2H), 3.28 (dt, *J* = 12.7, 3.3 Hz, 2H), 2.88 (td, *J* = 12.7, 3.1 Hz, 2H), 2.05 (dddd, *J* = 14.2, 8.0, 6.4, 3.0 Hz, 1H), 1.90 (dd, *J* = 14.2, 3.5 Hz, 2H), 1.57 – 1.41 (m, 2H). LCMS (ESI m/z): 210.1 (M+H).

Synthesis of Compound 2 (Table 1)

4-(3-(1-methylpiperidin-4-yl)-1,2,4-oxadiazol-5-yl)phenol (2). To a solution of compound **3** (400 mg, 1.6 mmol) and 37% HCHO (0.26 mL) in water (5.0 mL) was added AcOH (0.3 mL) followed by addition of $NaBH_3CN$ (200 mg, 3.18 mmol). The mixture was stirred at room temperature for 1 h. It was quenched with aq. $NaHCO_3$ and concentrated to give the crude

product, which was purified by prep-HPLC (FA) to give the desired product (160 mg, 38%). ^{1}H NMR (400 MHz, CD_3OD) δ 8.52 (br, 1H), 7.98 (d, *J* = 6.8 Hz, 2H), 6.96 (d, *J* = 6.8 Hz, 2H), 3.51-3.48 (m, 2H), 3.20-3.18 (m, 3H), 2.85 (s, 3H), 2.37-2.32 (m, 2H), 2.17-2.14 (m, 2H). LCMS (ESI m/z): 259.9 (M+H)

4-(3-(piperidin-4-yl)-1,2,4-oxadiazol-5-yl)phenol (3). To a solution of **35** (345 mg, 1.0 mmol) in EtOAc (3.0 mL) was added HCl/EtOAc (5.0 mL). The formed mixtre was stirred for 1 h at room temperature. Solvent was removed to give the desired product (280 mg, 99%). ^{1}H NMR (400 MHz, CD_3OD) *δ* 7.96 (d, *J* = 6.8 Hz, 2H), 6.93 (d, *J* = 6.8 Hz, 2H), 3.49-3.46 (m, 2H), 3.25-3.19 (m, 3H), 2.30 (m, 2H), 2.08-2.06 (m, 2H). LCMS (ESI m/z): 246.4 (M+H)

Compounds 4 and 5 were prepared in a manner similar to compound 2 (Scheme 1)

4-(3-(1-methylpyrrolidin-3-yl)-1,2,4-oxadiazol-5-yl)phenol (4). ^{1}H NMR (500 MHz, DMSO-d6) δ 7.93 – 7.89 (m, 2H), 6.97 – 6.92 (m, 2H), 3.55 – 3.47 (m, 1H), 2.94 – 2.89 (m, 1H), 2.69 – 2.61 (m, 2H), 2.58 – 2.53 (m, 1H), 2.30 (s, 3H), 2.26 – 2.17 (m, 1H), 2.12 – 2.03 (m, 1H). LCMS (ESI m/z): 246.4 (M+H).

4-(3-(pyrrolidin-3-yl)-1,2,4-oxadiazol-5-yl)phenol (5). ^{1}H NMR (500 MHz, DMSO-d6) δ 10.47 (s, 1H), 9.22 (s, 1H), 7.99 – 7.89 (m, 2H), 7.03 – 6.93 (m, 2H), 3.78 (p, *J* = 7.6 Hz, 1H), 3.64 (dd, *J* = 8.2, 11.7 Hz, 1H), 3.41 (dd, *J* = 7.4, 11.7 Hz, 1H), 3.39 – 3.25 (m, 2H), 2.45 – 2.36 (m, 1H), 2.26 – 2.14 (m, 1H). LCMS (ESI m/z): 232.4 (M+H).

Synthesis of Compound 6 (Scheme 2)

4-(4-(piperidin-4-yl)oxazol-2-yl)phenol (6). A mixture of *tert*-butyl 4-(2-(4-methoxyphenyl)oxazol-4-yl)piperidine-1-carboxylate (**37**, 0.1 g, 0.3 mmol) and hydrobromic acid (2 mL) was heated to 120º C for 16 h under a nitrogen atmosphere. After cooling to room temperature, the mixture was concentrated in vacuo. The crude residue was purified by reverse

phase chromatography (hydrochloric acid) to give the title compound (70 mg, 80%) as a white solid. ^{1}H NMR (400 MHz, DMSO-d_6) δ 9.15 (s, 1H), 8.85 (s, 1H), 7.89 (s, 1H), 7.74 (d, J = 8.4 Hz, 2H), 6.87 (d, J = 8.4 Hz, 2H), 3.28 - 3.23 (m, 2H), 3.01 - 2.91 (m, 2H), 2.85 - 2.79 (m, 1H), 2.07 - 2.04 (m, 2H), 1.82 - 1.72 (m, 2H). LCMS (ESI m/z) 245.4.

4-(5-(piperidin-4-yl)oxazol-2-yl)phenol (7). A mixture of *tert*-butyl 4-(2-(4-methoxyphenyl)oxazol-5-yl)piperidine-1-carboxylate (**42,** 0.4 g, 1.06 mmol) and hydrobromic acid (10 mL) was heated to 120º C for 6 h under a nitrogen atmosphere. After cooling to room temperature, the mixture was concentrated in vacuo. The crude residue was purified by reverse phase chromatography (formic acid) to give the title compound (66 mg, 24%) as a white solid. ^{1}H NMR (400 MHz, DMSO-d6) δ 10.09 (s, 1H), 9.18 (d, J = 9.5 Hz, 1H), 8.87 (d, J = 10.7 Hz, 1H), 7.91 (d, J = 1.0 Hz, 1H), 7.82 – 7.73 (m, 2H), 6.94 – 6.86 (m, 2H), 3.29 (dt, J = 12.8, 3.1 Hz, 2H), 2.99 (dtd, J = 12.7, 9.9, 2.7 Hz, 2H), 2.86 (tdd, J = 11.4, 10.4, 4.0, 2.0 Hz, 1H), 2.09 (dd, J = 14.3, 3.6 Hz, 2H), 1.88 – 1.73 (m, 2H). LCMS (ESI m/z): 245.4 (M+H).

4-(5-(piperidin-4-yl)oxazol-2-yl)phenol (8). Prepared in a manner similar to example 7. ^{1}H NMR (400 MHz, DMSO-d_6) δ 8.36 (s, 1H), 7.75 - 7.68 (m, 1H), 7.00 (s, 1H), 6.73 - 6.65 (m, 2H), 3.22 - 3.15 (m, 2H), 3.04 - 2.98 (m, 1H), 2.90 - 2.83 (m, 2H), 2.05 - 2.00 (m, 2H), 1.74 - 1.63 (m, 2H). LCMS (ESI m/z): 263.3 (M+H).

4-[5-(4-hydroxyphenyl)-3-pyridyl]phenol (17). Prepared in a manner similar to **18.** ^{1}H NMR (400 MHz, DMSO-d6) δ 9.66 (s, 2H), 8.71 (d, J = 2.2 Hz, 2H), 8.09 (t, J = 2.2 Hz, 1H), 7.69 – 7.60 (m, 4H), 6.94 – 6.85 (m, 4H). LCMS (ESI m/z): 264.5 (M+H).

Synthesis of Compound 18 (Scheme 4)

4-[2,6-diamino-5-(4-hydroxyphenyl)-3-pyridyl]phenol (18): Into a 500-mL 3-necked round-bottom flask purged and maintained with an inert atmosphere of nitrogen was placed a

solution of **44** (12 g, 59.68 mmol, 1.00 equiv) in CH_3CN (100 mL), (4-methoxyphenyl)boronic acid (11 g, 72.39 mmol, 1.20 equiv), Na_2CO_3(120 mL, sat.), and $Pd(dppf)_2Cl_2$ (1.2 g, 1.64 mmol, 0.03 equiv). The resulting solution was stirred at 110º C for 1 h, diluted with of 500 mL of EtOAc and then extracted 2 X 500 mL with EtOAc. The combined organic layers were washed 3 X 200 mL with brine, dried over anhydrous sodium sulfate and concentrated under vacuum. The crude residue was carried forward without further purification.

The crude residue was dissolved in dichloromethane (100 mL) and charged with tribromoborane (19.6 g, 78.24 mmol, 3.00 equiv) at 0º C. The resulting solution was stirred at room temperature for 1 h and then quenched by the addition of 100 mL of $NaHCO_3$ (1M) at 0º C. The solids were collected by filtration and then washed with 1x100 mL of H_2O and 1 X 300 mL of EtOAc/PE (1:1) to afford 6.3 g (83%) of the title compound as a white solid. ^{1}H NMR (400 MHz, DMSO-d6) δ 9.34 (s, 2H), 7.24 – 7.15 (m, 4H), 6.89 (s, 1H), 6.83 – 6.74 (m, 4H), 5.06 (s, 4H). ^{13}C NMR (101 MHz, DMSO-d6) δ 156.23, 154.35, 139.83, 129.86, 115.98, 110.55. LCMS (ESI m/z): 294.1 (M+H).

Compounds 19 -23 were prepared according to the synthesis of 18 (Scheme 4)

4-[6-amino-5-(4-hydroxyphenyl)-4-methyl-3-pyridyl]phenol (19). ^{1}H NMR (400 MHz, DMSO-d6) δ 9.48 (s, 2H), 8.14 (s, 1H), 7.71 (s, 1H), 7.14 – 7.00 (m, 4H), 6.92 – 6.84 (m, 2H), 6.84 – 6.75 (m, 2H), 4.95 (s, 2H), 1.81 (s, 3H). LCMS (ESI m/z): 293.0 (M+H).

4-[6-amino-4-ethyl-5-(4-hydroxyphenyl)-3-pyridyl]phenol (20). ^{1}H NMR (400 MHz, DMSO-d6) δ 9.48 (s, 2H), 8.14 (s, 1H), 7.65 (s, 1H), 7.13 – 7.00 (m, 4H), 6.92 – 6.83 (m, 2H), 6.84 – 6.75 (m, 2H), 4.90 (s, 2H), 2.24 (q, J = 7.4 Hz, 2H). LCMS (ESI m/z): 306.1 (M+H).

4-[6-amino-5-(4-hydroxyphenyl)-4-propyl-3-pyridyl]phenol (21). ^{1}H NMR (400 MHz, DMSO-d6) δ 13.80 (s, 1H), 9.82 (s, 1H), 9.70 (s, 1H), 7.77 (s, 1H), 7.22 – 7.04 (m, 6H), 7.00 – 6.88 (m, 2H), 6.91 – 6.79 (m, 2H), 1.04 (h, *J* = 7.3 Hz, 2H). LCMS (ESI m/z): 321.1 (M+H).

4-[6-amino-5-(4-hydroxyphenyl)-4-isopropyl-3-pyridyl]phenol (22). ^{1}H NMR (400 MHz, DMSO-d6) δ 9.48 (s, 2H), 8.14 (s, 1H), 7.58 (s, 1H), 7.09 – 6.97 (m, 5H), 6.92 – 6.83 (m, 2H), 6.81 – 6.73 (m, 2H), 2.87 (p, *J* = 7.2 Hz, 1H), 0.79 (d, *J* = 7.2 Hz, 7H). LCMS (ESI m/z): 321.1 (M+H).

2-amino-3,5-bis(4-hydroxyphenyl)pyridine-4-carbonitrile (23). ^{1}H NMR (400 MHz, DMSO-d6) δ 9.75 (s, 2H), 8.15 (s, 1H), 8.09 (s, 1H), 7.37 – 7.29 (m, 2H), 7.30 – 7.21 (m, 2H), 6.95 – 6.81 (m, 4H), 5.86 (s, 2H). LCMS (ESI m/z): 304.1 (M+H).

Compounds 24 - 27 were prepared according to the synthesis of compound 28 (Scheme 5)

4-(2-amino-4-ethyl-5-phenyl-3-pyridyl)phenol (24). ^{1}HNMR (400 MHz, DMSO-d6) δ 9.52 (s, 1H), 7.70 (s, 1H), 7.46 – 7.27 (m, 6H), 7.10 – 7.02 (m, 2H), 6.93 – 6.84 (m, 2H), 5.01 (s, 2H), 3.27 (s, 2H), 2.26 (q, *J* = 7.4Hz, 2H), 0.61 (t, J = 7.4 Hz, 3H). LCMS (ESI m/z): 291.1 (M+H).

3-[6-amino-4-ethyl-5-(4-hydroxyphenyl)-3-pyridyl]benzonitrile (25). ^{1}HNMR(400MHz, DMSO-d6) δ 9.54 (s, 1H), 7.81 (dd, *J* = 7.3, 1.5Hz, 2H), 7.77 – 7.52 (m, 4H), 7.13 – 7.01 (m, 2H), 6.93 – 6.85 (m, 2H), 5.10 (s, 2H), 3.28 (s, 2H), 2.24 (q, *J* = 7.4Hz, 2H), 0.60 (t, *J* = 7.5Hz, 3H). LCMS (ESI m/z): 316.1 (M+H).

4-[2-amino-4-ethyl-5-(1H-indazol-6-yl)-3-pyridyl]phenol (26). ^{1}H NMR (400 MHz, DMSO-d6) δ 13.07 – 13.02 (m, 1H), 9.55 (s, 1H), 8.09 (s, 1H), 7.81 – 7.74 (m, 2H), 7.42 (d, *J* = 1.3 Hz, 1H), 7.07 (td, *J* = 8.3, 1.7 Hz, 3H), 6.94 – 6.84 (m, 2H), 5.12 (s, 2H), 2.29 (q, *J* = 7.4 Hz, 2H), 0.62 (t, *J* = 7.4 Hz, 3H). LCMS (ESI m/z): 331.1 (M+H).

5-[6-amino-4-ethyl-5-(4-hydroxyphenyl)-3-pyridyl]-N-methyl-pyridine-2-carboxamide (27): ^{1}H NMR (400 MHz, DMSO-d6) δ 9.56 (s, 1H), 8.80 (q, *J* = 4.7 Hz, 1H), 8.59 (dd, *J* = 2.3, 0.9 Hz, 1H), 8.07 (dd, *J* = 8.0, 0.9 Hz, 1H), 7.96 (dd, *J* = 8.0, 2.2 Hz, 1H), 7.79 (s, 1H), 7.11 – 7.02 (m, 2H), 6.94 – 6.86 (m, 2H), 5.19 (s, 2H), 2.84 (d, *J* = 4.8 Hz, 3H), 2.26 (q, *J* = 7.4 Hz, 2H), 0.62 (t, *J* = 7.4 Hz, 3H). LCMS (ESI m/z): 349.1 (M+H).

4-[2-amino-4-ethyl-5-(1H-indazol-5-yl)-3-pyridyl]phenol (28): Into a 250-mL 3-necked round-bottom flask purged and maintained with an inert atmosphere of nitrogen was placed **50** (1.0 g, 3.41 mmol, 1.00 equiv), 6-(tetramethyl-1,3,2-dioxaborolan-2-yl)-2H-indazole (880 mg, 3.41 mmol, 1.00 equiv), potassium carbonate (3.3 g, 23.88 mmol, 7.00 equiv), water (30 mL), 1,4-dioxane (25 mL), and $Pd(dppf)_2Cl_2$ (200 mg, 0.3 mmol, 0.1 equiv). The resulting solution was stirred at 80º C for 16 h, diluted with 500 mL of H_2O and 500 mL of ethyl acetate. The organic layer was washed twice with 250 mL of brine and concentrated under vacuum. The residue was purified on a silica gel column eluting with DCM/CH_3OH (20:1-10:1) to afford the title compound. ^{1}H NMR (400 MHz, DMSO-d6) δ 13.07 (s, 1H), 9.52 (s, 1H), 8.07 (d, *J* = 1.0 Hz, 1H), 7.74 (s, 1H), 7.65 (dd, J = 1.6, 0.8 Hz, 1H), 7.56 (dt, *J* = 8.6, 0.9 Hz, 1H), 7.28 (dd, *J* = 8.5, 1.6 Hz, 1H), 7.10 – 7.04 (m, 2H), 6.92 – 6.86 (m, 2H), 4.94 (s, 2H), 2.26 (q, *J* = 7.4 Hz, 2H), 0.60 (t, *J* = 7.4 Hz, 3H). LCMS (ESI m/z): 331.1 (M+H).

4-[2-amino-4-ethyl-5-(2-methylindazol-6-yl)-3-pyridyl]phenol (29): Prepared according to the synthesis of **28.** Refer to Kategaya et al. for spectral information [1]

Synthesis of Compound 30 (Scheme 6)

4-(6-amino-4-ethyl-5-phenyl-3-pyridyl)phenol (30): A solution of 4-(6-amino-5-bromo-4-ethylpyridin-3-yl)phenol (59 mg, 0.2 mmol) in 0.5 ml of 1,4-dioxane was charged with phenylboronic acid (36 mg, 0.3 mmol),bis(diphenylphosphino)ferrocene]dichloropalladium(II)

(14 mg, 0.02 mmol), and 0.5 ml of 1M K_2CO_3. The mixture was then heated at 120º C for 5 minutes. The mixture was then diluted with ethyl acetate and water. The layers were separated and the organic layer was washed once with water, dried over Na_2SO_4, filtered, and concentrated in vacuo. The residue was then purified by reverse-phase preparatory HPLC to afford the title compound (29 mg, 50% yield). ^{1}H NMR (400 MHz, DMSO-d6) δ 9.39 (s, 1H), 7.70 (s, 1H), 7.56 – 7.46 (m, 2H), 7.46 – 7.35 (m,1H), 7.30 – 7.22 (m, 2H), 7.14 – 7.06 (m, 2H), 6.84 – 6.75 (m, 2H), 4.90 (s, 2H), 2.22 (q, *J* = 7.5 Hz, 2H), 0.61 (t, *J* = 7.4 Hz, 3H). LCMS (ESI m/z): 291.0 (M+H).

Compounds 31 and 32 were prepared according to the synthesis of compound 30 (Scheme 6)

3-[2-amino-4-ethyl-5-(4-hydroxyphenyl)-3-pyridyl]benzonitrile (31). ^{1}H NMR (400 MHz, DMSO-d6) δ 9.43 (s, 1H), 7.87 (dt, *J* = 7.7, 1.5 Hz, 1H), 7.78 – 7.63 (m, 4H), 7.61 (dt, *J* = 7.8, 1.5 Hz, 1H), 7.15 – 7.02 (m, 3H), 6.86 – 6.76 (m, 3H), 5.19 (s, 3H). LCMS (ESI m/z): 316.0 (M+H).

4-[6-amino-4-ethyl-5-(1H-indazol-5-yl)-3-pyridyl]phenol (32). ^{1}H NMR (400 MHz, DMSO-d6) δ 13.14 (s, 1H), 9.42 (s, 1H), 8.14 (s, 1H), 8.10 (d, *J* = 0.9 Hz, 1H), 7.70 (s, 1H), 7.70 – 7.62 (m, 2H), 7.19 (dd, *J* = 8.3, 1.7 Hz, 1H), 7.16 – 7.00 (m, 2H), 6.85 – 6.75 (m, 2H), 4.97 (s, 2H). LCMS (ESI m/z): 331.1 (M+H).

tert-butyl 4-(5-(4-hydroxyphenyl)-1,2,4-oxadiazol-3-yl)piperidine-1-carboxylate (35). To a solution of compound **33** (2.1 g, 10 mmol) in EtOH (5 mL) was added aqueous NH_4OH (1.5 mL, 50%). The mixture was heated at reflux for 70 min. The mixture was concentrated *in vacuo* to give the crude product, which was used for the next step directly. A mixture of compound **34** (2.14 g, 10 mmol) and CDI (1.62 g, 10 mmol) in DMF (5.0 mL) was stirred for 0.5 hour at room

temperature. Then to this mixture was added the above crude product, and the mixture was heated to 110º C for 2 h. Solvent was removed *in vacuo* and the crude product was purified by silica gel column chromatography (DCM/CH_3OH=30/1) to afford the desired product as a white solid (345 mg, 10%). ^{1}H NMR (400 MHz, CD_3OD) δ 7.98 (d, J = 6.8 Hz, 2H), 6.95 (d, J = 6.8 Hz, 2H), 4.13-4.10 (m, 2H), 3.36-3.32 (m, 3H), 2.04 (m, 2H), 1.82-1.73 (m, 2H), 1.50 (s, 9H). LCMS (ESI m/z): 245.5 [M+H].

tert-butyl 4-(2-(4-methoxyphenyl)oxazol-4-yl)piperidine-1-carboxylate (37). A mixture of 4-methoxybenzamide (0.5 g, 3.31 mmol) and *tert*-butyl 4-(2-bromoacetyl)piperidine-1-carboxylate (**36**, 2.03 g, 6.62 mmol) in toluene (10 mL) was heated to 100º C for 16 h under a nitrogen atmosphere. After cooling to room temperature, the mixture was concentrated in vacuo. The crude residue was purified by silica gel chromatography to give the title compound (0.1 g, 8%) as a white solid. ^{1}H NMR (400 MHz, DMSO-d_6) δ 9.15 (s, 1H), 8.85 (s, 1H), 7.89 (s, 1H), 7.74 (d, J = 8.4 Hz, 2H), 6.87 (d, J = 8.4 Hz, 2H), 3.28 - 3.23 (m, 2H), 3.01 - 2.91 (m, 2H), 2.85 - 2.79 (m, 1H), 2.07 - 2.04 (m, 2H). LCMS (ESI m/z): 246.4 (M+H)

***tert*-butyl-4-(1-hydroxy-2-nitroethyl)piperidine-1-tert-butyl-4-(1-hydroxy-2-nitroethyl)piperidine-1-carboxylatecarboxylate (39).** To a solution of *tert*-butyl 4-formylpiperidine-1-carboxylate (**38**, 20 g, 93.8 mmol) and nitromethane (11.45 g, 187 mmol) in THF (100 mL) and *t*-BuOH (100 mL) was added *t*-BuOK (10.52 g, 93.8 mmol). The mixture was stirred at room temperature for 2 h. The mixture was acidified with AcOH to pH 6 and then extracted with EtOAc (100 mL × 3). The combined organic layers were washed with brine (100 mL), dried over anhydrous Na_2SO_4 and concentrated in vacuo. The crude residue was purified by silica gel chromatography to give the title compound (16 g, 62%) as a faint yellow solid. ^{1}H NMR (400 MHz, DMSO-d_6) δ 4.19 - 4.01 (m, 2H), 3.28 - 3.24 (m, 1H), 2.89 - 2.86 (m, 1H),

2.55 - 2.64 (m, 2H), 2.22 - 2.13 (m, 4H), 1.84 - 1.79 (m, 1H), 1.56 - 1.41 (m, 2H), 1.43 (s, 9H), 1.28 - 1.17 (m, 2H). LCMS (ESI m/z): 275.4 (M+H).

***tert*-butyl 4-(2-amino-1-hydroxyethyl)piperidine-1-carboxylate (40).** To a solution of *tert*-butyl 4-(1-hydroxy-2-nitroethyl)piperidine-1-carboxylate (**39,** 16 g, 58 mmol) in MeOH (25 mL) was added 10% Pd/C (1.6 g). The mixture was stirred at room temperature for 12 h under a hydrogen atmosphere (50 psi). The mixture was filtered and the filtrate was concentrated in vacuo to give the title compound (12 g, crude) as a yellow solid that required no further purification. ^{1}H NMR (400 MHz, DMSO-d_6) δ 5.41 (d, J = 6.4 Hz, 1H), 4.76 - 4.72 (m, 1H), 4.40 - 4.34 (m, 1H), 3.95 - 3.89 (m, 3H), 2.70 - 2.52 (m, 2H), 1.69 - 1.65 (m, 1H), 1.55 - 1.52 (m, 2H), 1.39 (s, 9H), 1.23 - 1.10 (m, 2H). LCMS (ESI m/z): 246.4 (M+H).

***tert*-butyl 4-(4-methoxybenzamido)acetyl)piperidine-1-carboxylate (41).** To a solution of 4-methoxybenzoic acid (1.5 g, 8.8 mmol) and *tert*-butyl 4-(2-amino-1-hydroxyethyl)piperidine-1-carboxylate (**40**, 2.58 g, 10.58 mmol) in DMF (20 mL) was added HATU (6.7 g, 17.63 mmol) and triethylamine (3.67 mL, 26.45 mmol). The mixture was stirred at room temperature for 6 h. The mixture was concentrated in vacuo. The crude residue was purified by silica gel chromatography (petroleum ether / EtOAc = 1 : 1) to give *tert*-butyl 4-(2-(2-fluoro-4-methoxybenzamido)-1-hydroxyethyl)piperidine-1-carboxylate(1.78 g, 51%) as a faint yellow solid.

To a solution of *tert*-butyl 4-(4-methoxybenzamido)-1-hydroxyethyl)piperidine-1-carboxylate (1.2 g, 3.03 mmol) in DCM (20 mL) was added Dess-Martin reagent (3.2 g, 7.55 mmol). The mixture was stirred at room temperature for 4 h. The mixture was concentrated in vacuo. The crude residue was purified by silica gel chromatography to give the title compound (1.1 g, 92%) as a white solid. ^{1}H NMR (400 MHz, DMSO-d_6) δ 7.84 - 7.79 (m, 1H), 7.66 -7.61 (m, 1H),

6.89 - 6.80 (m, 2H), 4.02 - 3.93 (m, 2H), 3.73 (s, 3H), 3.41 - 3.36 (m, 2H), 3.16 - 3.09 (m, 1H), 2.59 - 2.51 (m, 2H), 1.72 - 1.68 (m, 2H), 1.52 - 1.45 (m, 2H), 1.35 (s, 9H). LCMS (ESI m/z): 377.2.4 (M+H).

***tert*-butyl 4-(2-(4-methoxyphenyl)oxazol-5-yl)piperidine-1-carboxylate (42).** To a solution of *tert*-butyl 4-(2-(2(4-methoxybenzamido)acetyl)piperidine-1-carboxylate (0.5 g, 1.27 mmol) in THF (20 mL) was added Burgess reagent (906 mg, 3.8 mmol). The mixture was heated to 60º C for 6 h under a nitrogen atmosphere. After cooling to room temperature, the mixture was concentrated in vacuo. The crude residue was purified by silica gel chromatography to give the title compound (0.4 g, 84%) as a white solid. ^{1}H NMR (400 MHz, DMSO-d_6) δ 8.36 (s, 1H), 7.75 - 7.68 (m, 1H), 7.00 (s, 1H), 6.73 - 6.65 (m, 2H), 3.22 - 3.15 (m, 5H), 3.04 - 2.98 (m, 1H), 2.90 - 2.83 (m, 2H), 2.05 - 2.00 (m, 2H), 1.74 - 1.63 (m, 2H), 1.40 – 1.25 (m, 9H). LCMS (ESI m/z): 358.4 (M+H).

3,5-dibromopyridine-2,6-diamine (44, R1 and R2 = NH2, R3 = H): Into a 500-mL 3-necked round-bottom flask purged and maintained with an inert atmosphere of nitrogen was placed 4-ethylpyridin-2-amine (10 g, 81.85 mmol, 1.00 equiv), tetrahydrofuran (200 mL), and NBS (29 g, 162.94 mmol, 2.00 equiv) at 0º C. The resulting solution was stirred at room temperature for 15 min and then 5 concentrated under vacuum. The residue was purified on a silica gel column eluting with DCM/MeOH (100:1-20:1) to afford 18 g (79%) of 3,5-dibromo-4-ethylpyridin-2-amine as a white solid. ^{1}H NMR (400 MHz, Chloroform-*d*) δ 8.04 (s, 1H), 7.33 – 7.23 (m, 1H), 4.93 (s, 2H), 2.93 (q, J = 7.5 Hz, 2H), 1.17 (t, J = 7.5 Hz, 3H). LCMS (ESI m/z): 246.4 (M+H).

3,5-dibromo-4-ethylpyridin-2-amine (46): Into a 500-mL 3-necked round-bottom flask purged and maintained with an inert atmosphere of nitrogen was placed 4-ethylpyridin-2-amine

(10 g, 81.85 mmol, 1.00 equiv), tetrahydrofuran (200 mL), and NBS (29 g, 162.94 mmol, 2.00 equiv) at 0º C. The resulting solution was stirred at room temperature for 15 min and then 5 concentrated under vacuum. The residue was purified on a silica gel column eluting with DCM/MeOH (100:1-20:1) to afford 18 g (79%) of the title compound. ^{1}H NMR (400 MHz, Chloroform-*d*) δ 8.04 (s, 1H), 4.93 (s, 2H), 2.93 (q, *J* = 7.5 Hz, 2H), 1.17 (t, *J* = 7.5 Hz, 3H). LCMS (ESI m/z): 278.9 (M+H).

3-bromo-4-ethylpyridin-2-amine (47): Into a 500-mL 3-necked round-bottom flask purged and maintained with an inert atmosphere of nitrogen was placed **45** (18 g, 64.29 mmol, 1.00 equiv) in tetrahydrofuran (300 mL). To this was added a solution of n-BuLi (in hexane) (58 mL, 2.00 equiv, 2.2 mol/L) at -78º C. The resulting solution was stirred at -78º C for 1 h, quenched by the addition of 450 mL of NH_4Cl and then extracted with 2 X 500 mL of ethyl acetate. The combined organic layers were washed with 2X 500 mL of brine, dried over anhydrous sodium sulfate and concentrated under vacuum. The crude product was purified by Flash-Prep-HPLC to afford 12 g (93%) of the title compound as a white solid. ^{1}H NMR (400 MHz, Chloroform-*d*) δ 7.89 (d, *J* = 5.1 Hz, 1H), 6.60 – 6.48 (m, 1H), 4.93 (s, 2H), 2.69 (q, *J* = 7.6 Hz, 2H), 1.33 – 1.14 (t, *J* = 7.5 Hz, 3H). LCMS (ESI m/z): 201.0 (M+H).

4-ethyl-3-(4methoxyphenyl)pyridn-2-amine (48): Into a 500-mL 3-necked round-bottom flask purged and maintained with an inert atmosphere of nitrogen was placed a solution of 3-bromo-4-ethylpyridin-2-amine (12 g, 59.68 mmol, 1.00 equiv) in CH_3CN (100 mL), (4-methoxyphenyl)boronic acid (11 g, 72.39 mmol, 1.20 equiv), Na_2CO_3(120 mL, sat.), and $Pd(dppf)_2Cl_2$ (1.2 g, 1.64 mmol, 0.03 equiv). The resulting solution was stirred at 110º C for 1 h, diluted with of 500 mL of EA and then extracted with of 2 X 500 mL of ethyl acetate. The combined organic layers were washed with 3x200 mL of brine, dried over anhydrous sodium

sulfate and concentrated under vacuum. The residue was purified on a silica gel column eluting with ethyl acetate/petroleum ether (1:100-1:10) to afford 10 g (73%) of the title compound. ^{1}H NMR (400 MHz, Chloroform-*d*) δ 8.06(d, *J* = 5.1 Hz, 1H), 7.21 – 7.11 (m, 2H), 7.06 – 6.97 (m, 2H), 6.64 (d, *J* = 5.4 Hz, 1H), 4.48 (s, 2H), 3.86 (s, 3H), 2.31 (q, *J* = 7.6 Hz, 2H), 1.11 – 0.88 (t, *J* = 7.5 Hz, 3H). LCMS (ESI m/z): 229.1 (M+H).

5-bromo-4-ethyl-3-(4-methoxyphenyl)pyridin-2-amine (49): Into a 250-mL 3-necked round-bottom flask purged and maintained with an inert atmosphere of nitrogen was placed 4-ethyl-3-(4methoxyphenyl)pyridn-2-amine (10 g, 43.80 mmol, 1.00 equiv), tetrahydrofuran (100 mL), followed by NBS (7.8 g, 43.83 mmol, 1.00 equiv) at 0º C. The resulting solution was stirred at room temperature for 15 min, diluted with 500 mL of EtOAc and 500 mL of H_2O. The resulting solution was extracted with 2x500 mL of ethyl acetate. The organic layers were combined, washed with 2x500 mL of brine and concentrated under vacuum. The residue was purified on a silica gel column eluting with ethyl acetate/petroleum ether (1:20-1:10) to afford 8 g (59%) of the title compound. ^{1}H NMR (400 MHz, Chloroform-*d*) δ 8.09 (s, 1H), 7.22 – 7.09 (m, 2H), 7.09 – 6.98 (m, 2H), 4.55 (s, 2H), 2.47 (q, *J* = 7.5 Hz, 2H), 1.10 – 0.84 (t, *J* = 7.5 Hz, 3H). LCMS (ESI M/Z): 307.1 (M+H).

4-(2-amino-5-bromo-4-ethylpyridin-3-yl)phenol (50): Into a 250-mL 3-necked round-bottom flask purged and maintained with an inert atmosphere of nitrogen was placed 5-bromo-4-ethyl-3-(4-methoxyphenyl)pyridin-2-amine as a white solid (8 g, 26.04 mmol, 1.00 equiv), dichloromethane (100 mL), followed by tribromoborane (19.6 g, 78.24 mmol, 3.00 equiv) at 0º C. The resulting solution was stirred at room temperature for 1 h and then quenched by the addition of 100 mL of 1M $NaHCO_3$ at 0º C. The solids were collected by filtration and then washed with 1x100 mL of H_2O and 1x300 mL of EA/PE (1:1) to afford 6.3 g (83%) of 4-(2-

amino-5-bromo-4-ethylpyridin-3-yl)phenol as a white solid. ^{1}H NMR (400 MHz, Chloroform-*d*) δ 8.09 (s, 1H), 7.22 – 7.09 (m, 2H), 7.09 – 6.98 (m, 2H), 4.55 (s, 2H), 2.47 (q, *J* = 7.5 Hz, 2H), 1.10 – 0.84 (t, *J* = 7.5 Hz, 3H). LCMS (ESI m/z): 293.0 (M+H).

5-bromo-4-ethyl-pyridin-2-amine (52): A solution of 4-ethyl-pyridine-2-amine (**50**, 10 g, 82 mmol) in 300 ml of THF was cooled to 0º C and charged with N-Bromosuccinimide (14.7 g, 82 mmol). The mixture was then stirred at 0º C for an additional 15 minutes. The mixture was then concentrated down and the residue was purified by silica-gel chromatography (0-5% MeOH in DCM) to afford 20 5-bromo-4-ethylpyridin-2-amine **16a** (12 g, 72% yield). ^{1}H NMR (400 MHz, Chloroform-*d*) δ 8.08 (d, *J* = 0.5 Hz, 1H), 7.32 – 7.21 (m, 1H), 6.40 (q, *J* = 0.6 Hz, 1H), 4.36 (s, 2H), 2.62 (qd, *J* = 7.5, 0.7 Hz, 2H), 1.21 (t, *J* = 7.5 Hz, 3H). LCMS (ESI m/z): 201. (M+H).

4-ethyl-5-(4-methoxyphenyl)pyridin-2-amine (53): A solution of 5-bromo-4-ethylpyridin-2-amine (**52**, 1.0 g, 5.0 mmol) in 12 ml of acetonitrile was charged with 4-methoxy-boronic acid (907 mg, 6.0 mmol), bis(diphenylphosphino)ferrocene]dichloropalladium(II) (364 mg, 0.5 mmol), and 12 ml of 1 M Potassium Carbonate. The mixture was then heated at 120º C for 5 minutes. The mixture was then diluted with ethyl acetate and water. The layers were separated aqueous and the organic layer was washed once with water, dried over Na_2SO_4, filtered, and concentrated *in vacuo*. The residue was then purified by silica-gel chromatography (1-15% MeOH in DCM) to afford 4-ethyl-5-(4-methoxyphenyl)pyridin-2-amine (900 mg, 3.9 mmol, 80%). ^{1}H NMR (400 MHz, Chloroform-*d*) δ 7.80 (s, 1H), 7.23 – 7.10 (m, 2H), 7.00 – 6.86 (m, 3H), 4.94 (s, 2H), 3.85 (s, 3H), 2.67 (q, *J* = 7.5 Hz, 2H), 1.05 (t, *J* = 7.5 Hz, 3H). LCMS (ESI m/z): 229.1 (M+H).

3-bromo-4-ethyl-5-(4-methoxyphenyl)pyridin-2-amine (54): A solution of 5-bromo-4-ethylpyridin-2-amine (9.5 g, 42 mmol) in 100 ml of THF was charged with N-Bromosuccinimide

(7.5 g, 42 mmol) and stirred at room temperature for 15 minutes. The mixture was then concentrated *in vacuo* and the residue was purified by silica-gel chromatography (0-5% MeOH in DCM) to afford the title compound (8.6 g, 67% yield). ^{1}H NMR (400 MHz, Chloroform-*d*) δ 7.80 (s, 1H), 7.23 – 7.10 (m, 2H), 7.00 – 6.86 (m, 2H), 4.94 (s, 2H), 3.85 (s, 3H), 2.67 (q, J = 7.5 Hz, 2H), 1.05 (t, J = 7.5 Hz, 3H). LCMS (ESI m/z): 307.0 (M+H).

4-(6-amino-5-bromo-4-ethylpyridin-3-yl)phenol (55): A solution of 3-bromo-4-ethyl-5-(4-methoxyphenyl)pyridin-2-amine (**54**, 6.6 g, 21 mmol) in 40 ml of THF was charged with 64 ml of 1 M Boron Tribromide in DCM. After stirring at room temperature for 15 minutes, the mixture was then cooled 0º C and charged with 100 ml of saturated sodium carbonate. The layers were separated and the organic was dried over Mg_2SO_4, filtered, and concentrated in vacuo to afford 4-(6-amino-5-bromo-4-ethylpyridin-3-yl)phenol (5.7 g, 90% yield). ^{1}H NMR (400 MHz, Chloroform-*d*) δ 7.80 (s, 1H), 7.23 – 7.10 (m, 2H), 7.00 – 6.86 (m, 2H), 4.94 (s, 2H), 2.67 (q, J = 7.5 Hz, 2H), 1.05 (t, J = 7.5 Hz, 3H). LCMS (ESI m/z): 293.1 (M+H).

ASSOCIATED CONTENT

Supporting Information. This material is available free of charge via the Internet at http://pubs.acs.org.

Table S1 (word file): Compounds lacking phenol in C3/C5 position

Table S2 (word file): Crystallography data collection and refinement statistics

Figure S1 (word file): Computational torsion scan results

Molecular formula strings and biochemical data (CSV)

^{1}H and ^{13}C 1D NMR spectra of all synthesized compounds (pdf)

AUTHOR INFORMATION

Corresponding Authors

*Phone: +1-650- 467-4914. E-mail: dilellop@gene.com

* Phone: +1-650-225-8114. E-mail: pastor.richard@gene.com

*Phone: +1-650-534-8426. E-mail: vickie.tsui@aya.yale.edu

Author Contributions

The manuscript was written through contributions of all authors. All authors have given approval to the final version of the manuscript. ‡P.D.L. and R.P. contributed equally.

ACKNOWLEDGMENT

The authors thank Michael Hayes for compound purification, and Baiwei Lin for analytical support. We also thank the Genentech Biomolecular Resources group. Use of the Stanford Synchrotron Radiation Lightsource, SLAC National Accelerator Laboratory, is supported by the U.S. Department of Energy, Office of Science, Office of Basic Energy Sciences under Contract No. DE-AC02-76SF00515. The SSRL Structural Molecular Biology Program is supported by the DOE Office of Biological and Environmental Research, and by the National Institutes of Health, National Institute of General Medical Sciences (including P41GM103393). The contents of this

publication are solely the responsibility of the authors and do not necessarily represent the official views of NIGMS or NIH.

ABBREVIATIONS

DUBs, deubiquitinating enzymes; USP, ubiquitin-specific protease; UCH, ubiquitin C-terminal hydrolase; OTU, ovarian tumor protease; HAUSP, herpes virus associated USP; NMR, nuclear magnetic resonance; USP7-CD, USP7-catalytic domain; STD, saturation transfer difference; TROSY, Transverse Relaxation Optimized SpectroscopY; HTS, high-throughput screening; SAR, structure-activity relationship.

PDB ID codes: **5WHC** (crystal structure of **2** in complex with USP7-CD), **5WH7** (crystal structure of **16** with USP7-CD). Authors will release the atomic coordinates and experimental data upon article publication.

REFERENCES

(1) Kategaya, L.; Di Lello, P.; Rouge, L.; Pastor, R.; Clark, K. R.; Drummond, J.; Kleinheinz, T.; Lin, E.; Upton, J. P.; Prakash, S.; Heideker, J.; McCleland, M.; Ritorto, M. S.; Bainbridge, T. W.; Ma, T. P.; Kwok, M.; Stiffler, Z.; Brasher, B.; Alessi, D. R.; Trost, M.; Tang, Y.; Jaishanker, P.; Hearn, B.; Renslo, A. R.; Arkin, M. R.; Cohen, F.; Yu, K.; Peale, F.; Gnad, F.; Chang, M. T.; Klijn, C.; Blackwood, E.; Martin, S. E.; Forrest, W. F.; Ernst, J. A.; Ndubaku, C.; Wang, X.; Berensini, M. H.; Tsui, V.; Schwerdtfeger, C.; Blake, R. A.; Murray, J.; Maurer, T.;

Wertz, I. E. USP7 small molecule inhibitors interfere with ubiquitin binding. *Nature* **2017,** *550*, 534-538.

(2) Hochstrasser, M. Ubiquitin-dependent protein degradation. *Annu. Rev. Genet.* **1996,** *30*, 405-439.

(3) Ardley, H. C.; Robinson, P. A. E3 ubiquitin ligases. *Essays Biochem.* **2005,** *41*, 15-30.

(4) Pickart, C. M.; Fushman, D. Polyubiquitin chains: polymeric protein signals. *Curr. Opin. Chem. Biol.* **2004,** *8*, 610-616.

(5) Komander, D.; Rape, M. The ubiquitin code. *Annu. Rev. Biochem.* **2012,** *81*, 203-229.

(6) Komander, D.; Clague, M. J.; Urbe, S. Breaking the chains: structure and function of the deubiquitinases. *Nat. Rev. Mol. Cell Biol.* **2009,** *10*, 550-563.

(7) Liang, J.; Saad, Y.; Lei, T.; Wang, J.; Qi, D.; Yang, Q.; Kolattukudy, P. E.; Fu, M. MCP-induced protein 1 deubiquitinates TRAF proteins and negatively regulates JNK and NF-kappaB signaling. *J. Exp. Med.* **2010,** *207*, 2959-2973.

(8) Fraile, J. M.; Quesada, V.; Rodriguez, D.; Freije, J. M.; Lopez-Otin, C. Deubiquitinases in cancer: new functions and therapeutic options. *Oncogene* **2012,** *31*, 2373-2388.

(9) Abdul Rehman, S. A.; Kristariyanto, Y. A.; Choi, S. Y.; Nkosi, P. J.; Weidlich, S.; Labib, K.; Hofmann, K.; Kulathu, Y. MINDY-1 is a member of an evolutionarily conserved and structurally distinct new family of deubiquitinating enzymes. *Mol. Cell.* **2016,** *63*, 146-155.

(10) Daviet, L.; Colland, F. Targeting ubiquitin specific proteases for drug discovery. *Biochimie* **2008,** *90*, 270-283.

(11) Lim, K. H.; Baek, K. H. Deubiquitinating enzymes as therapeutic targets in cancer. *Curr. Pharm. Des.* **2013,** *19*, 4039-4052.

(12) Becker, K.; Marchenko, N. D.; Palacios, G.; Moll, U. M. A role of HAUSP in tumor suppression in a human colon carcinoma xenograft model. *Cell Cycle* **2008,** *7*, 1205-1213.

(13) Levine, A. J. p53, the cellular gatekeeper for growth and division. *Cell* **1997,** *88*, 323-331.

(14) Hollstein, M.; Sidransky, D.; Vogelstein, B.; Harris, C. C. p53 mutations in human cancers. *Science* **1991,** *253*, 49-53.

(15) Brown, C. J.; Lain, S.; Verma, C. S.; Fersht, A. R.; Lane, D. P. Awakening guardian angels: drugging the p53 pathway. *Nat. Rev. Cancer.* **2009,** *9*, 862-873.

(16) Tovar, C.; Rosinski, J.; Filipovic, Z.; Higgins, B.; Kolinsky, K.; Hilton, H.; Zhao, X.; Vu, B. T.; Qing, W.; Packman, K.; Myklebost, O.; Heimbrook, D. C.; Vassilev, L. T. Small-molecule MDM2 antagonists reveal aberrant p53 signaling in cancer: implications for therapy. *Proc. Natl. Acad. Sci. U S A* **2006,** *103*, 1888-1893.

(17) Ammirati, M.; Bagley, S. W.; Bhattacharya, S. K.; Buckbinder, L.; Carlo, A. A.; Conrad, R.; Cortes, C.; Dow, R. L.; Dowling, M. S.; El-Kattan, A.; Ford, K.; Guimaraes, C. R.; Hepworth, D.; Jiao, W.; LaPerle, J.; Liu, S.; Londregan, A.; Loria, P. M.; Mathiowetz, A. M.; Munchhof, M.; Orr, S. T.; Petersen, D. N.; Price, D. A.; Skoura, A.; Smith, A. C.; Wang, J. Discovery of an in Vivo Tool to Establish Proof-of-Concept for MAP4K4-Based Antidiabetic Treatment. *ACS Med. Chem. Lett.* **2015,** *6*, 1128-33.

(18) Ohki, H.; Ota, M.; Shibata, Y.; Watanabe, H.; Motoki, R.; Tominaga, Y.; Jimbo, T. Preparation of bicyclic pyrimidine-carboxamide compounds as inhibitors of receptor tyrosine kinase Axl. *WO 2013162061A1* **2013**.

(19) Lau, W. C. Novel Fyn kinase inhibitors for therapeutic applications. *WO 2017044623 A1* **2017**.

(20) Ndubaku, C.; Tsui, V. Inhibiting the deubiquitinating enzymes (DUBs). *J. Med. Chem.* **2015,** *58*, 1581-1595.

(21) Feng, J. A.; Aliagas, I.; Bergeron, P.; Blaney, J. M.; Bradley, E. K.; Koehler, M. F.; Lee, M. L.; Ortwine, D. F.; Tsui, V.; Wu, J.; Gobbi, A. An integrated suite of modeling tools that empower scientists in structure- and property-based drug design. *J. Comput. Aided Mol. Des.* **2015,** *29*, 511-523.

(22) Rougé, L.; Bainbridge, T. W.; Kwok, M.; Tong, R.; Di Lello, P.; Wertz, I. E.; Maurer, T.; Ernst, J. A.; Murray, J. Molecular understanding of USP7 substrate recognition and C-terminal activation. *Structure* **2016,** *24*, 1335-1345.

(23) Di Lello, P.; Rougé, L.; Pan, B.; Maurer, T. (1)H, (13)C and (15)N backbone resonance assignment for the 40.5 kDa catalytic domain of Ubiquitin Specific Protease 7 (USP7). *Biomol. NMR Assign.* **2016,** *10*, 345-349.

(24) Mayer, M.; Meyer, B. Characterization of ligand binding by saturation transfer difference NMR spectroscopy. *Angewandte Chemie-International Edition* **1999,** *38*, 1784-1788.

(25) Pervushin, K.; Riek, R.; Wider, G.; Wuthrich, K. Attenuated T2 relaxation by mutual cancellation of dipole– dipole coupling and chemical shift anisotropy indicates an avenue to

NMR structures of very large biological macromolecules in solution. *Proc. Natl. Acad. Sci. U S A* **1997,** *94*, 12366-12371.

(26) Delaglio, F.; Grzesiek, S.; Vuister, G. W.; Zhu, G.; Pfeifer, J.; Bax, A. NMRPipe: A multidimensional spectral processing system based on UNIX pipes. *J. Biomol. NMR* **1995,** *6*, 277-293.

(27) Johnson, B. A.; Blevins, R. A. NMRView: A computer program for the visualization and analysis of NMR data. *J. Biomol. NMR* **1994,** *4*, 603-614.

Table 1. Active-site binder and biochemically active hits from virtual screening

Cmpd	Structure	USP7 IC_{50} (μM)
1	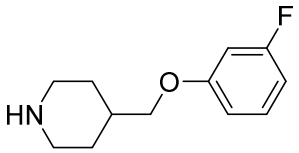	>2000
2	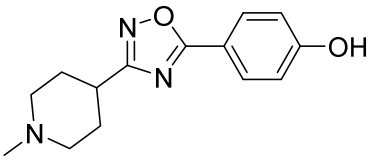	79.2
3	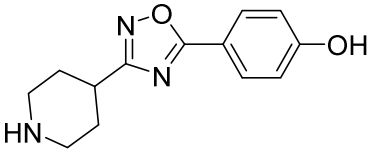	97.7
4	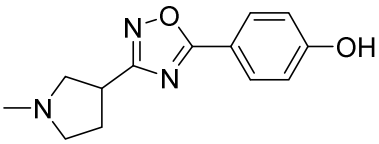	131
5	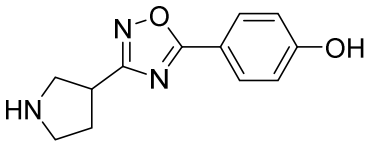	132

Table 2. Structure-based optimization of the oxadiazole series

Cmpd	Structure	USP7 IC_{50} (μM)
6	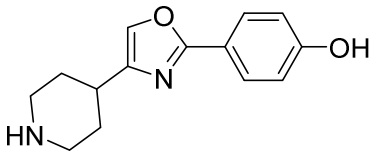	85.2
7	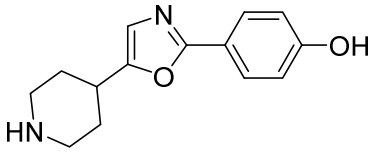	32.8
8	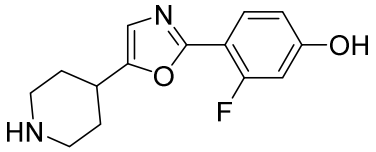	18.4

Table 3. Phenol substituted aminopyridines from HTS hits

Cmpd	Structure	USP7 IC_{50} (μM)
14	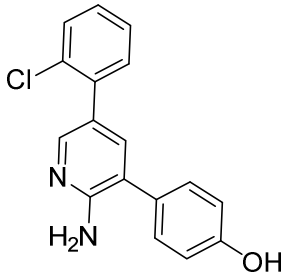	33.2
15	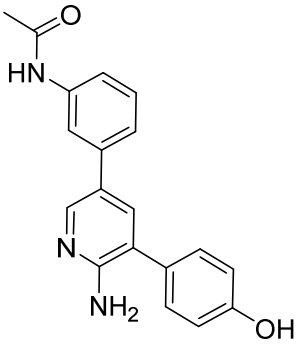	15.1
16*	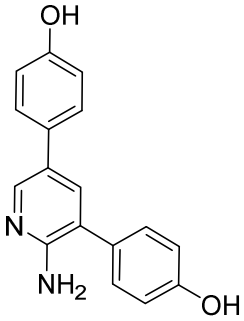	11.1

*Not screened in HTS

Table 4. C2, C4, and C6 substituent SAR

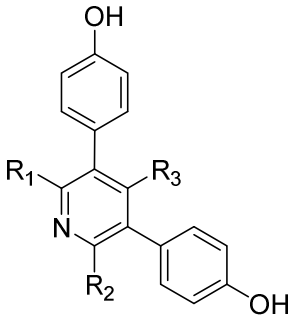

Cmpd	R1	R2	R3	USP7 IC_{50} (μM)
17	H	H	H	>50
18	NH_2	NH_2	H	8.5
19	H	NH_2	CH_3	7.6
20	H	NH_2	C_2H_5	2.5
21	H	NH_2	C_3H_7	13.6
22	H	NH_2	iPr	21.4
23	H	NH_2	CN	>200

Table 5. SAR at the C3 and C5 positions

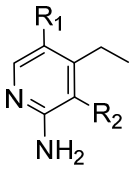

Cmpd	R1	R2	USP7 IC_{50} (μM)
24	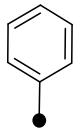	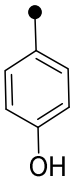	9.6
25	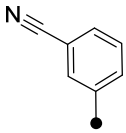	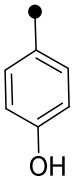	2.5
26	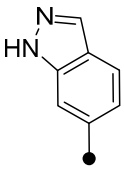	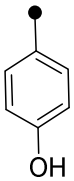	0.48
27	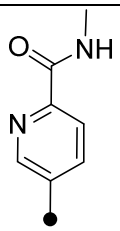	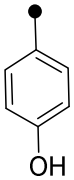	1.34
28	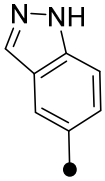	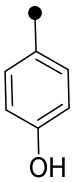	0.75
29	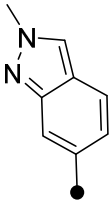	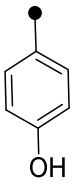	>63.3

Cmpd	R1	R2	USP7 IC_{50} (μM)
30	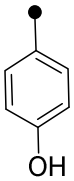	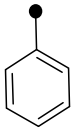	22.4
31	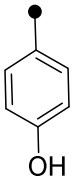	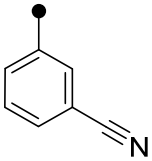	5.2
32	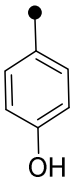	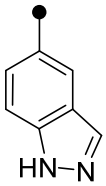	0.61

Table 6. MDM2 MSD cell-based assay data for selected compounds

Cmpd	EC_{50} (μM)
18	36.5
27	2.58
28	0.3
29	>50
31	37.5

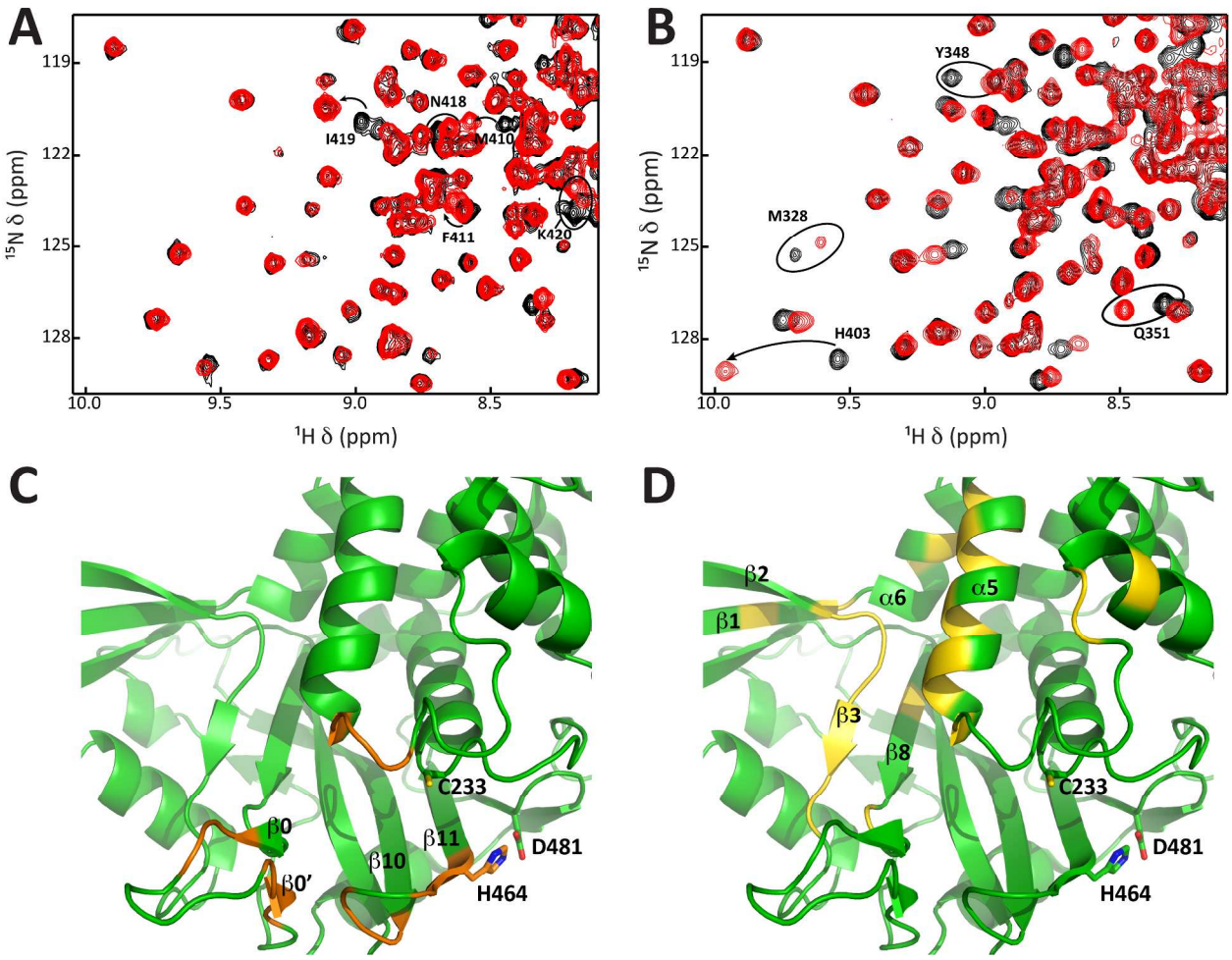

Figure 1. Compound **1** and compound **2** bind two distinct sites on USP7-CD. (A) Selected region of the overlay between the 2D ^{1}H-^{15}N TROSY spectra of labeled USP7-CD apo (in black) and in the presence of eight equivalents of compound **1** (in red). (B) Selected region of the overlay between the 2D ^{1}H-^{15}N TROSY spectra of labeled USP7-CD apo (in black) and after addition of eight equivalents of compound **2** (in red). Arrows and ovals indicate signals undergoing large chemical shifts changes. (C-D) Ribbon model of the apo USP7-CD crystal structure (PDB code 4M5W). Amino acids experiencing large chemical shifts perturbations upon formation of the USP7-CD/**1** complex are highlighted in orange, whereas the amino acids

displaying large chemical shifts changes upon formation of the USP7-CD/**2** complex are colored in yellow. The catalytic triad residues, Cys223, His464 and Asp481, are shown in sticks.

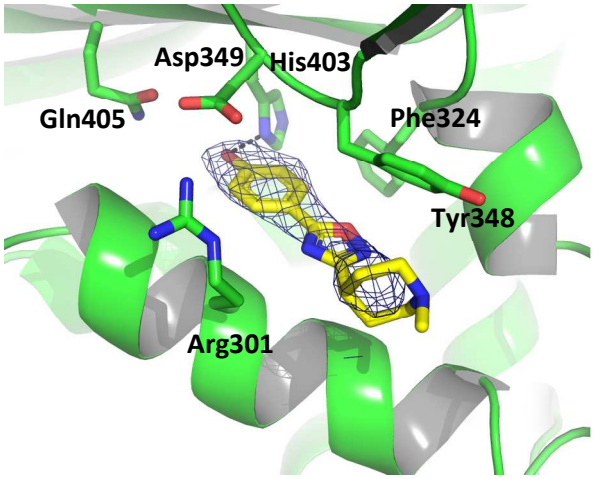

Figure 2. Crystal structure of **2** in complex with USP7-CD (PDB code 5WHC). Blue mesh represents electron density contoured at 0.7σ.

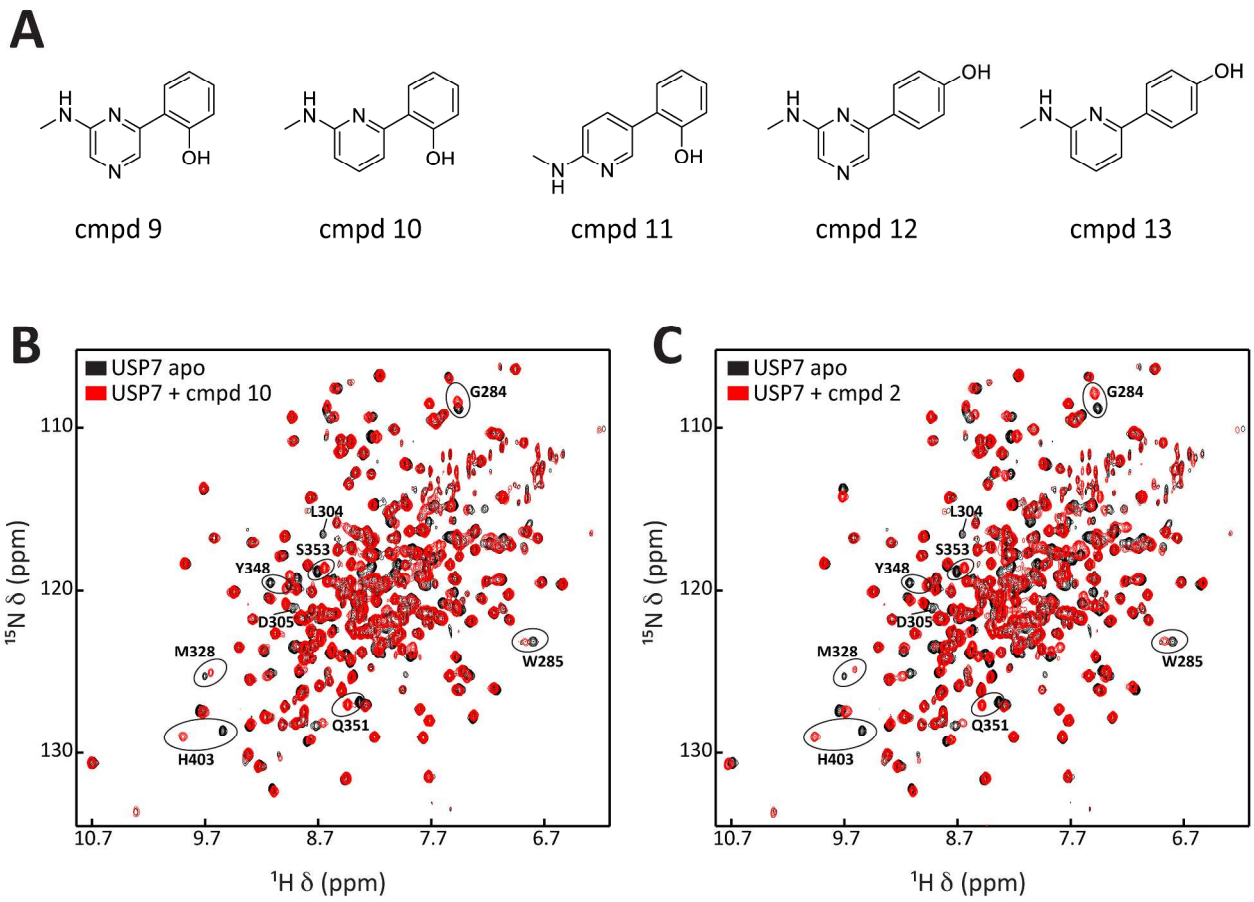

Figure 3. Compound **2** and compound **10** bind to the same site on USP7-CD. (A) Re-mined fragment hits from the NMR screen. (B) 2D ^{1}H-^{15}N TROSY spectra overlay for labeled USP7-CD in the apo form (in black) and in the presence of compound **10** (in red). Protein:ligand ratio 1:8. (C) Overlay between the 2D ^{1}H-^{15}N TROSY spectra of labeled USP7-CD apo (in black) and after addition of compound **2** (in red). Protein:ligand ratio 1:8. Arrows and ovals highlight some of the signals undergoing large chemical shifts changes or line broadening upon complex formation. The chemical shifts changes induced by the two distinct series are virtually identical.

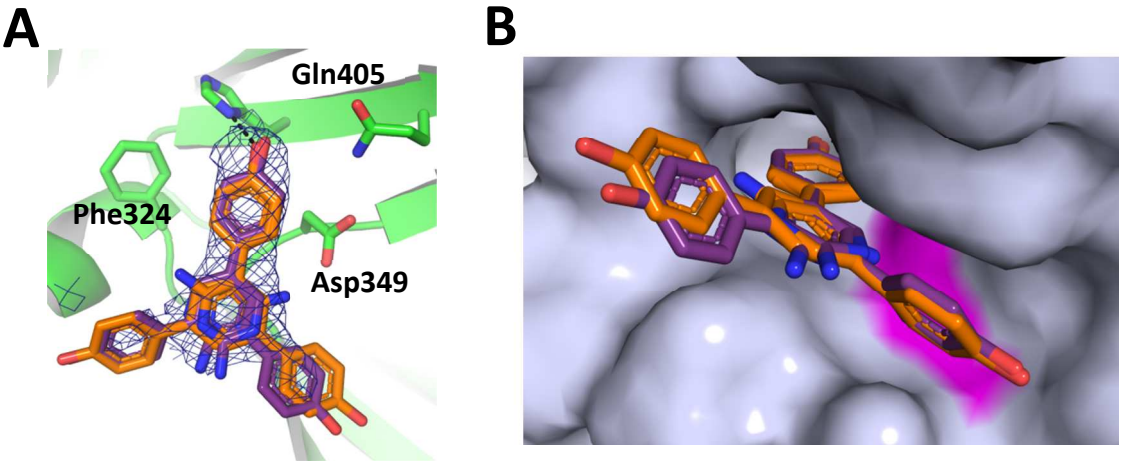

Figure 4. Co-crystal structure of **16** with USP7-CD (PDB Code 5WH7). **(A)** 2.8 Å Electron density (blue mesh) for **16** was ambiguous and suggested that it was possible to bind in different alternate conformations. **(B)** Surface representation of the binding pocket highlighting the hydrophobic pocket (magenta).

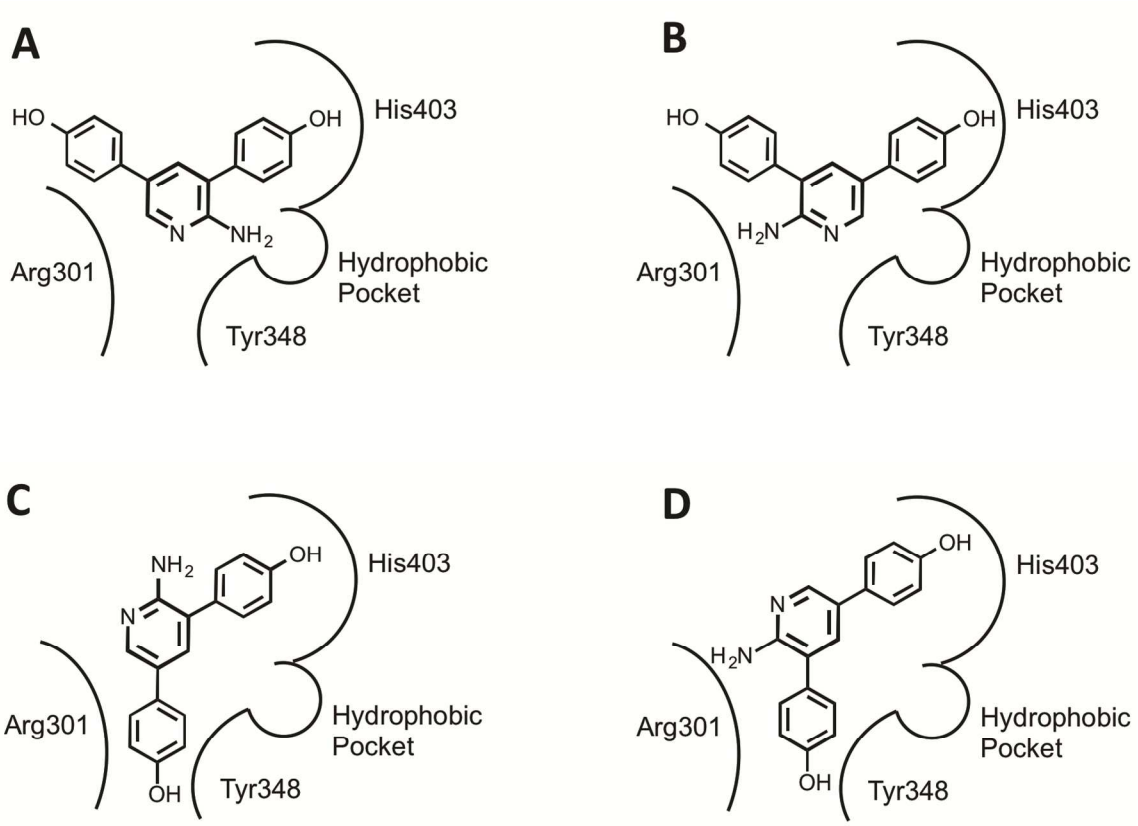

Figure 5. 2D Representation of possible ligand binding modes.

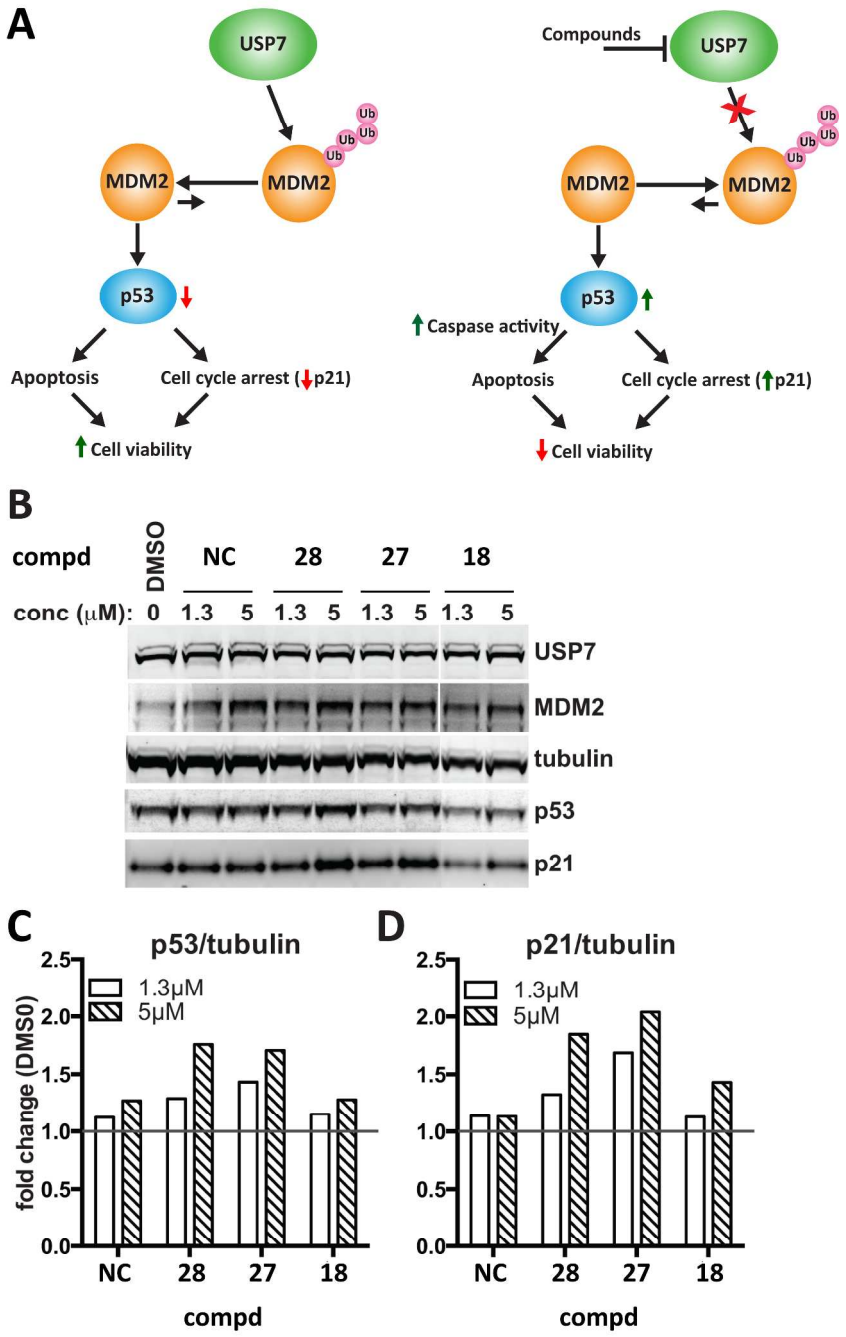

Figure 6. Inhibiting USP7 activity increases p53 and p21 levels of EOL-1 cells. **(A)** Illustration of USP7 signaling through the MDM2-p53-p21 axis in the absence (left panel) and in the presence (right panel) of USP7 inhibitors. Left panel: USP7 stabilizes MDM2 by rescuing it from proteosomal degradation. MDM2 down-regulates the p53 pathway thus leading to a

reduction in p53-depended apoptosis, a reduction in p21-mediated cell cycle arrest and an increase in cell viability. Right panel: USP7 inhibition is expected to promote MDM2 proteosomal degradation. This causes a reduction in the MDM2 levels and the consequent increase in p53 protein levels, ultimately resulting in the activation of caspases and modulation of p53-target genes, e.g. p21. An increase in caspase activity triggers apoptosis while an increase in p21 triggers cell cycle arrest. Both result in a decrease in cell viability and cell number. **(B)** Western blots using antibodies against USP7, MDM2, tubulin, p53 and p21. **(C-D)** Graphs showing quantification of p53 and p21 western blots normalized to tubulin. Under these conditions, compounds **27** and **28** increase relative p53 levels while **18**, **27** and **28** increase relative p21 levels. Data is representative of 2 experiments. NC: negative control.

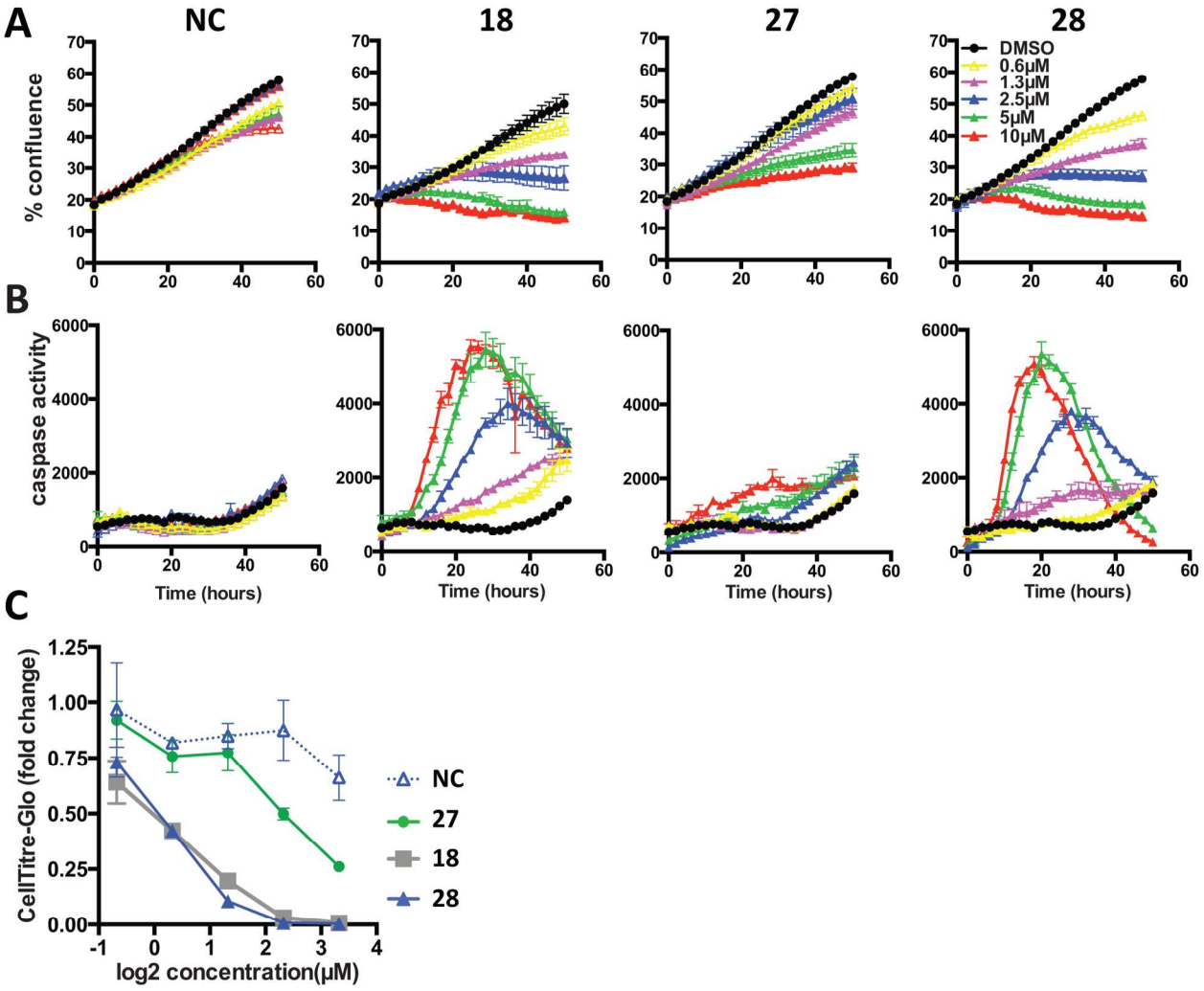

Figure 7. Inhibiting USP7 activity increases caspase activity and decreases viability of EOL-1 cells. **(A)** IncuCyte data showing a dose-dependent decrease in cell confluence with inhibitors relative to control. **(B)** IncuCyte data showing a dose-dependent increase in caspase activity with inhibitors relative to control. **(C)** CellTiter-Glo viability data validating IncuCyte cell confluence results. Data is representative of 3 experiments. NC: negative control.

Scheme 1. Synthesis of Compounds 2-3

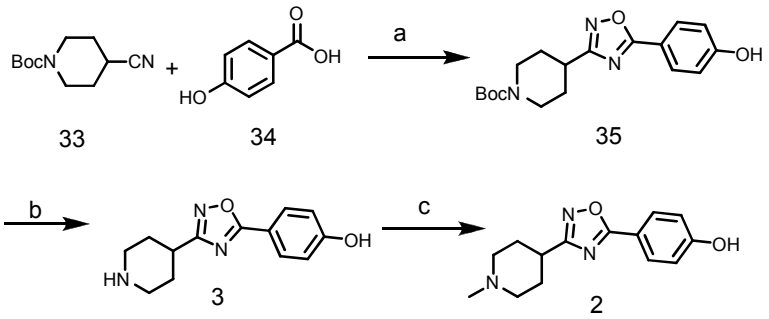

Reagents and Conditions. a) NH_2OH, CDI, 18% yield. b) HCl, EtOAc, 99% yield. c) HCHO, $NaCNBH_3$, AcOH, 38% yield

Scheme 2. Synthesis of Compound 6

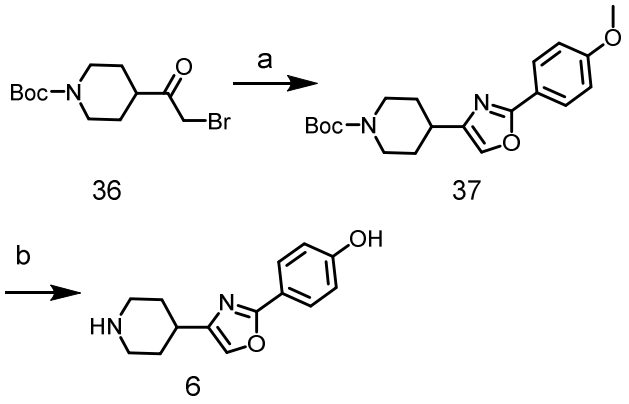

Reagents and Conditions. a) 4-OMe-Benzamide, 8% yield. b) HBr, 80% yield

Scheme 3. Synthesis of Compound 7

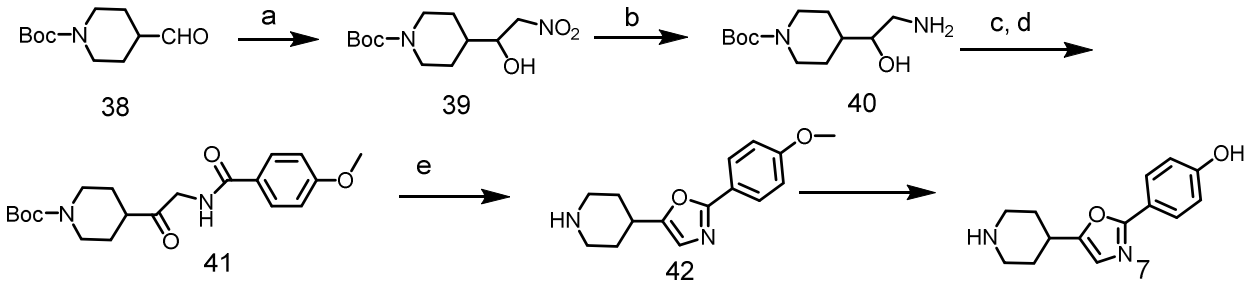

Reagents and Conditions. a) Nitromethane, KOtBu, 62% yield b) 10% Pd/C, H_2, quant. c) 4-OMe-Benzoic Acid, HATU, TEA, 51% yield d) Dess-Martin Reagent, 27% yield e) Burgess Reagent, 84% yield f) HBr, 24% yield

Scheme 4. Synthesis of Compounds 17 – 23

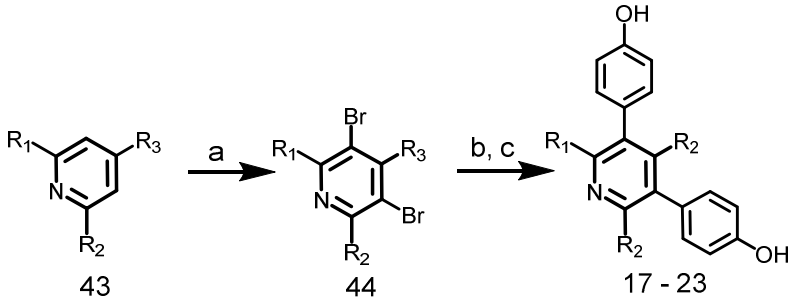

Reagents and Conditions. a) NBS, DCM. b) Anisole-4-Boronic Acid, $Pd(dppf)_2Cl_2$,Na_2CO_3, ACN, 120 ^oC, quant. c) BBr_3, DCM.

Scheme 5. Synthesis of Compounds 24 – 29

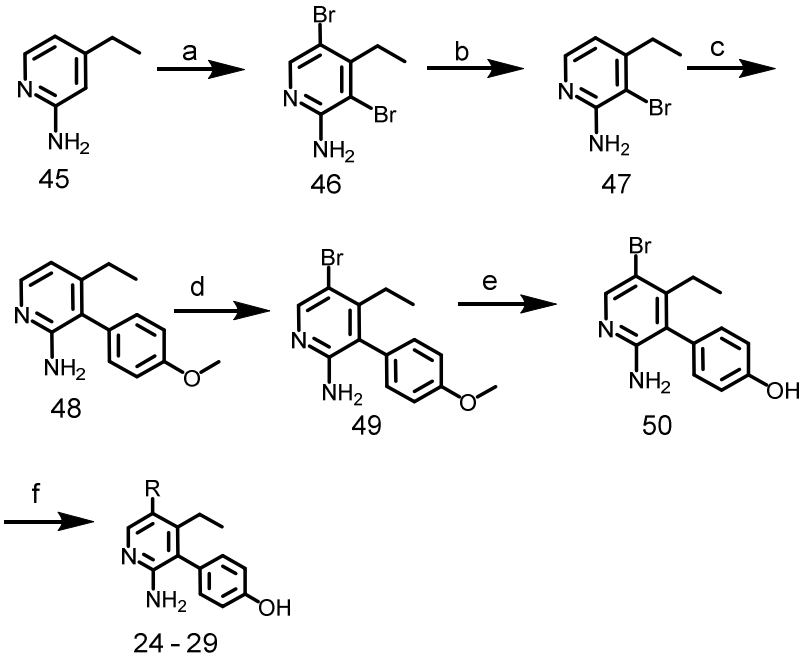

Reagents and Conditions. a) NBS, THF, 79% yield. b) n-BuLi, THF, -78 ^{o}C, 93% yield. c) Anisole-4-Boronic Acid, $Pd(dppf)_2Cl_2$, Na_2CO_3, ACN, 120 ^{0}C, 73% yield. d) NBS, DCM. 59% yield. e) BBr_3, DCM, 83% yield. f) $RB(OH)_2$, $Pd(dppf)_2Cl_2$, Na_2CO_3, ACN, 120 ^{0}C.

Scheme 6. Synthesis of Compounds 30-32

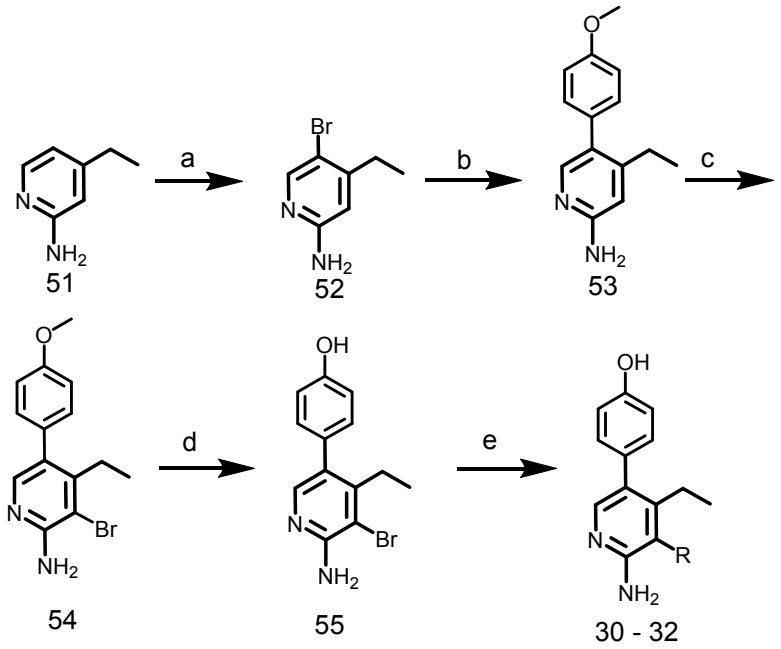

Reagents and Conditions. a) NBS, THF, 72% yield. b) Anisole-4-Boronic Acid, $Pd(dppf)_2Cl_2$,Na_2CO_3, ACN, 120^0C, 66% yield. c) NBS, TFH, 67% yield. d) BBr_3, DCM, 90% yield. e) $RB(OH)_2$, $Pd(dppf)_2Cl_2$, Na_2CO_3, ACN, 120 ^{0}C.

Table of Content Graphics